European Journal of Pharmaceutics and Biopharmaceutics 201 (2024) 114344

Contents lists available at ScienceDirect

European Journal of Pharmaceutics and Biopharmaceutics

journal homepage: www.elsevier.com/locate/ejpb

Research paper

Enantiospecific crystallisation behaviour of malic acid in mechanochemical reactions with vinpocetine

Ilenia D'Abbrunzo [a], Rebecca Birolo [b], Michele R. Chierotti [b], Dejan-Krešimir Bučar [c], Dario Voinovich [a], Beatrice Perissutti [a,*], Dritan Hasa [a,*]

[a] Department of Chemical and Pharmaceutical Sciences, University of Trieste, P.le Europa 1, 34127 Trieste, Italy
[b] Department of Chemistry and NIS Centre, University of Torino, V. Giuria 7, 10125 Torino, Italy
[c] Department of Chemistry, University College London, 20 Gordon Street, London WC1H 0AJ, UK

ARTICLE INFO

Keywords:
Chirality
Enantioselective crystallisation
Crystalline salt
Amorphous salt
Glass transition
Mechanochemistry

ABSTRACT

We report an intriguing example of enantioselectivity in the formation of new multicomponent crystalline solid containing vinpocetine and malic acid. Several experimental data sets confirmed that the multicomponent system presents a clear enantiospecific crystallisation behaviour both in the solid-state and in solution: only the system consisting of vinpocetine and L-malic acid produces a free-flowing solid consisting of a new crystalline form, while the experiments with D-malic acid produced an amorphous and often deliquescent material. The new vinpocetine-L-malic system crystallizes in the monoclinic space group of $P2_1$ and in a 1:1 molar ratio, where the two molecules are linked through intermolecular hydrogen bonds in the asymmetric unit. The vinpocetine-DL-malic system was partially crystalline (with also traces of unreacted vinpocetine) with diffraction peaks corresponding to those of vinpocetine-L-malic acid. Solid-state NMR experiments revealed strong ionic interactions in all the three systems. However, while vinpocetine-L-malic acid system was a pure and crystalline phase, the other two systems persistently showed the presence of unreacted vinpocetine. This resulted in a significant worsening of the dissolution profile with respect to the pure vinpocetine-L-malic crystalline salt, whose dissolution kinetics appeared superior.

1. Introduction

Chirality has recently been one of the most active topics in pharmaceutical materials science as it represents a distinctive feature found in many modern drugs [1,2]. The chirality of pharmaceutical compounds often governs medical treatments, directly affecting pharmacokinetic and pharmacodynamic parameters of drugs, thus having an impact on their potency and selectivity [2–7].

Multicomponent crystals containing chiral pharmaceutical compounds have been central for the understanding of enantiomer selectivity and regulation of the physicochemical properties of crystalline materials [8–11]. Since chirality represents a geometrical property, several chiral molecules often present difficulty on forming multicomponent crystalline solids with chiral coformers, thus showing an enantiospecific behaviour during crystallisation [12,13]. The enantiospecificity can be explained by the rather low stabilising energies present in these systems, which makes them particularly sensitive to changes in steric interactions and losses of stabilising secondary interactions that occur when chirality is reversed. In fact, a chirality inversion of the compounds to be crystallised usually leads to a variation of steric interactions and an alteration or loss of stabilising secondary interactions [14]. In this context, Springuel et al. reported that over 85 % of cocrystal systems found in the Cambridge Structural Database (CSD) show enantiospecificity. This statement comes from a meticulous

Abbreviations: VINPO, (S,S)-vinpocetine; L-MAL, L-malic acid; D-MAL, D-malic acid; DL-MAL, DL-malic acid; EA, ethyl acetate; EtOH, ethanol; AcT, acetone; ACN, acetonitrile; HXN, hexane; DSC, differential scanning calorimetry; PXRD, powder X-ray diffraction; SSNMR, solid-state NMR; SXRD, single-crystal X-ray diffraction; HSM, hot-stage microscopy; NG, neat grinding; LAG, liquid-assisted grinding, POLAG, polymer-assisted grinding; PEG, polyethylene glycol; VINPO-L-MAL, vinpocetine:L-malic acid; VINPO-L-MAL-NG, amorphous vinpocetine:L-malic acid obtained through neat grinding; VINPO-D-MAL, vinpocetine:D-malic acid; VINPO-DL-MAL, vinpocetine:DL-malic acid; VINPO-D-L-MAL PM, vinpocetine:DL-malic acid as physical mixtures of both enantiomers; ASU, asymmetric unit; T_g, glass transition; AUC, area under the curve.

* Corresponding authors.
E-mail addresses: bperissutti@units.it (B. Perissutti), dhasa@units.it (D. Hasa).

https://doi.org/10.1016/j.ejpb.2024.114344
Received 9 April 2024; Received in revised form 16 May 2024; Accepted 26 May 2024
Available online 28 May 2024

search in the CSD and from a cocrystal screening of chiral compounds (*i.e.*, levetiracetam, fasoracetam, dyprophylline, S-oxiracetam, 2R,3R-/2S,3S-tartaric acid, R-/S-mandelic acid, S-ibuprofen, S-3-phenyllactic acid, R-3-phenyllactic acid, S-phenylsuccinic acid, R-flurbiprofen, R-2-(4-hydroxyphenoxy)propionic acid, 1R,3S-camphoric acid, R-/S-methylsuccinic acid and stanozolol), which demonstrated that 11 out of 13 new cocrystals discovered exhibit enantiospecificity [14].

On this basis, our study explores the propensity of the chiral drug vinpocetine (14-ethoxycabonyl-(3α,16α-ethyl)-14,15-eburnamine) (Fig. 1a) to form multicomponent crystalline solids in the presence of a chiral coformer. Specifically, vinpocetine presents two stereogenic centers (C_3 and C_{16}) and is commercially available as (S,S)-vinpocetine (herein after referred to as VINPO) [15]. The drug is a synthetic derivative of vincamine (one of the main alkaloid molecules found in the *vinca minor* plant [16]), which is used for the treatment of cerebral disorders and diseases. It also increases the cerebral flow in the ischemic areas thus showing a neuroprotective effect against brain ischemia in patients with cerebrovascular diseases [17,18].

Pure VINPO, however, presents important biopharmaceutical limitations including a limited aqueous solubility and, consequently, a very low oral bioavailability [19]. It is therefore desirable producing a multicomponent system of such molecule with an improved dissolution profile.

In this work, malic acid (MAL) (1-hydroxy-1,2-ethanedicarboxylic acid) (Fig. 1b-c) was chosen as a salt forming agent [20], due to the low toxicity and because its common use as an excipient in the pharmaceutical and food industry [21,22].

Importantly, since both VINPO and MAL are chiral compounds, it was also possible to investigate the crystallisation of VINPO in the presence of each enantiomer (D-MAL and L-MAL) and the racemic form (DL-MAL).

The crystallisation tendency of these three systems (*i.e.*, VINPO-L-MAL, VINPO-D-MAL, VINPO-DL-MAL) was investigated using both solution-based and solid-state techniques, to understand if a change in the type of process and involved energies could lead to different outcomes in the formation of the multicomponent system.

As for the solution-based techniques, slow-evaporation crystallisation was used and, based on VINPO and MAL solubility values, different solvents were investigated. As for the solid-state techniques, three mechanochemical methods were used, namely neat grinding (NG), liquid-assisted grinding (LAG), and polymer-assisted grinding (POLAG). The crystal structure of VINPO-L-MAL system obtained through solution crystallisation was solved by single crystal X-ray diffraction (SXRD).

Furthermore, solid-state NMR (SSNMR) was performed to check the protonation state of VINPO in the three investigated systems as well as their crystallinity and purity. Finally, dissolution tests in non−sink conditions were performed at 37 C using a pH 7.4 phosphate buffer for the three VINPO-L-MAL, VINPO-D-MAL and VINPO-DL-MAL systems.

2. Materials and methods

2.1. Materials

VINPO of Ph. Eur. grade was purchased from Linnea (Locarno, Switzerland), while L-MAL, D-MAL, DL-MAL were provided from Sigma-Aldrich (St. Louis, USA). Hexane (HXN), ethyl acetate (EA), ethanol (EtOH), acetone (AcT), acetonitrile (ACN) and polyethylene glycol 3000 (PEG 3000) were purchased from Sigma-Aldrich (Milan, Italy). All the actives and chemicals were used as received.

2.2. Methods

2.2.1. Sample preparation

2.2.1.1. Solution crystallisation. Solution crystallisation experiments were performed at room temperature using four solvents namely, EA, EtOH, AcT and ACN. For each solvent, three vials consisting of a 1:1 M ratio of VINPO and the MAL enantiomer or the racemic compound were prepared. The approximate solubility values of VINPO and MAL and some chemical properties of the crystallisation solvents are reported in Table S1 in the Supplementary Information (SI) file. In the case of solution crystallisation in EA, 7.5 mg (0.021 mmol) of VINPO and 2.8 mg (0.021 mmol) of L-MAL/D-MAL/DL-MAL were transferred in a lidded vial (having an internal volume of 7 ml) and dissolved in 4 mL of solvent under continuous mixing with a magnetic stirrer for 45 min at room temperature. For the other three solvents (*i.e.*, EtOH, AcT, ACN), 20 mg (0.057 mmol) of VINPO and 7.6 mg (0.057 mmol) of the coformer were added and stirred for 45 min. Subsequently, the vials were pierced to enable slow solvent evaporation.

2.2.1.2. Mechanochemical screening experiments. The mechanochemical screening experiments were performed in Retsch MM200 vibrational mill (Retsch, Germany). The materials were processed using two 15 mL stainless steel jars containing two milling spheres with a diameter of 7 mm. Specifically, three mechanochemical methods were used, NG, LAG and POLAG [23].

NG experiments were performed by milling 200 mg of a mixture of VINPO and a coformer in a 1:1 M ratio for 60 min at 25 Hz. As for LAG, the drug-to-drug molar ratio, milling time and the milling frequency were kept fixed as NG experiments, while the same solvents of solution-

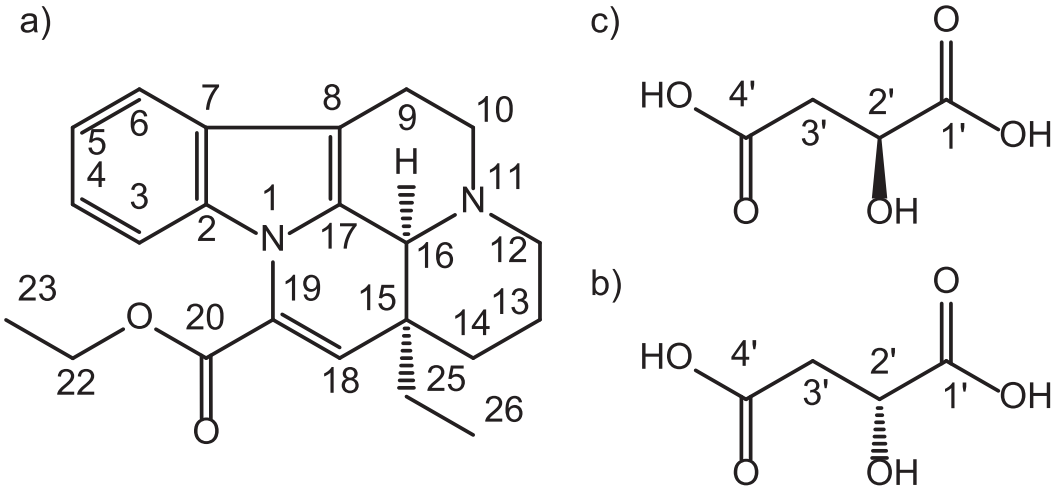

Fig. 1. (a) VINPO, (b) L-MAL and (c) D-MAL molecular structures with atom numbers (assigned for the solid-state NMR analysis).

based crystallisation processes (*i.e.*, EA, EtOH, AcT, ACN), plus hexane (HXN), were used in 4 different η values [24] ranging from 0.1 ($\mu L\ mg^{-1}$) to a maximum of 0.4 ($\mu L\ mg^{-1}$) since it is known from literature that for some systems different amounts of the same liquid can lead to different polymorphic forms [25] or can promote the amorphisation/crystallisation processes [26].

POLAG experiments were also performed, as polymers are known to accelerate and facilitate mechanochemical transformations [27]. Also, for such screening experiments, the drug-to-drug molar ratio, milling time and the frequency were kept fixed and used the same as those in NG and LAG experiments, while four δ values [28] ranging from 0.01 to 0.2 of PEG 3000 were tested.

The solid products were characterised by PXRD and DSC within 24 h after their preparation.

2.2.2. DSC analysis

The thermal behaviour of each system was characterised using a Mettler-Toledo DSC822e (Greifensee, Switzerland) connected to a cell Mettler DSC20 calorimeter, and operated with the STARe software. For each experiment, 2–4 mg of sample was weighed and introduced into an aluminium sealed and pierced crucible (internal volume of 40 μL). Samples were heated in the range 30–185 °C under an air atmosphere, using a heating rate of 10 °C min^{-1}.

DSC was also used to determine the glass transition (T_g) of amorphous materials. Specifically, T_g was obtained by heating each sample at 10 °C min^{-1} from 30 to 185 °C, quenching up to −20 °C at 50 °C min^{-1} and then re-heating, under nitrogen (N_2) flow. The T_g values were reported as inflection point of the curves.

2.2.3. PXRD analysis

PXRD experiments were carried out in a Bruker-AXS (Siemens), using CuKα source ($\lambda = 1.5418$ Å) with a voltage of 40 kV and an amperage of 30 mA. All the measurements were conducted at room temperature, in a 2θ range of 5-35° with a step-size of 0.05° and a time-step of 2 s.

2.2.4. Single crystal X-ray diffraction and crystal structure solution

The diffraction data for VINPO-L-MAL was collected on a four-circle *Agilent SuperNova* (Dual Source) single crystal X-ray diffractometer using a micro-focus CuKα X-ray beam ($\lambda = 1.54184$ Å) and a *HyPix-Arc 100* hybrid pixel array detector. The sample temperatures were controlled with an *Oxford Instruments* cryojet. All data were processed using the *CrysAlis^{Pro}* programme package from *Rigaku Oxford Diffraction* [29]. The crystal structures were solved with the *SHELXT* programme [30], used within the *Olex2* software suite [31], and refined by least squares on the basis of F^2 with the *SHELXL* programme [32] using the *ShelXle* graphical user interface [33]. All non-hydrogen atoms were refined anisotropically by the full-matrix least-squares method. Hydrogen atoms associated with carbon atoms were refined isotropically in geometrically constrained positions [$U_{iso}(H_C) = 1.2 \bullet U_{eq}(C)$, while hydrogen atoms affiliated with oxygen and nitrogen atoms were refined isotropically after being located in the difference map [$U_{iso}(H_{N,O}) = 1.5 \bullet U_{eq}(N,O)$]. Crystallographic and refinement parameters are reported in Table S2 in the SI file. An ORTEP plot of the content of the asymmetric unit is shown in Figure S5 in the same document.

2.2.5. Optical and hot-stage microscopy

Images of different VINPO-L-MAL single crystals were acquired through a ZEISS optical microscope equipped with long working distance objectives. Hot-stage microscopy (HSM) was also performed to confirm the melting temperature of the new system obtained: selected single crystals were heated from 30 °C to 170 °C with a heating rate of 10 °C min^{-1}, using a Mettler-Toledo Ltd. hot-stage microscopy apparatus (Greifensee, Switzerland).

2.2.6. SSNMR analysis

Solid-state NMR spectra were acquired with a Bruker Avance II 400 Ultra Shield instrument, operating at 400.23, 100.63 and 40.56 MHz for ^1H, ^{13}C and ^{15}N nuclei, respectively.

Powdered samples were packed into cylindrical zirconia rotors with a 4 mm o.d. and a 90 μL volume. A certain amount of sample was collected from each batch and used without further preparation to fill the rotor. ^{13}C CPMAS spectra were acquired at a spinning speed of 12 kHz, using a ramp cross-polarisation pulse sequence with a 90° ^1H pulse of 3.60 μs, a contact time of 3 ms, optimised recycle delays between 2.5 and 4.2 s, a number of scans in the range 600–2220, depending on the sample. ^{15}N CPMAS spectra were acquired at a spinning speed of 9 kHz using a ramp cross-polarisation pulse sequence with a 90° ^1H pulse of 3.60 μs, a contact time of 4 ms, optimised recycle delays between 2.5 and 4.2 s, a number of scans in the range 53880–115620, depending on the sample. For every spectrum, a two-pulse phase modulation (TPPM) decoupling scheme was used, with a radiofrequency field of 69.4 kHz. The ^{13}C and ^{15}N chemical shift scales were calibrated through the signals of γ-glycine (^{13}C methylenic peak at 43.7 ppm and ^{15}N peak at 33.4 ppm with reference to NH_3) as an external standard.

2.2.7. In vitro dissolution tests

In vitro dissolution kinetics of pure VINPO, VINPO-L-MAL, VINPO-D-MAL and VINPO-DL-MAL were carried out under non-sink conditions ($C > 0.2\ C_s$). Each experiment was performed using 150 mL of pH 7.4 phosphate buffer solution in a vessel directly connected to a thermostatic bath (37 °C), with a constant agitation provided by a magnetic stirrer. Under such conditions the solubility of pure VINPO is 1.6 mg L^{-1} [34]. Therefore, the equivalent of 5 mg of VINPO (maximum theoretical concentration of 33.3 mg L^{-1}) was added to the dissolution medium and the absorbance was measured in-situ through a fiber optic apparatus (HELLMA, Italy) connected to a spectrophotometer (ZEISS, Germany). The absorbance values were recorded at the maximum wavelength of the drug (270 nm) [35]. A Tyndall − Rayleigh scattering correction was applied to the recorded spectra to exclude the scattering occurring at every wavelength of undissolved particles. The results are reported as the average of three replicates.

3. Results and discussion

The crystallisation tendency of VINPO in the presence of L-MAL, D-MAL and DL-MAL was investigated both through solution crystallisations (slow evaporation) and mechanochemistry. In the case of VINPO-L-MAL system, single crystals (of different quality, depending on the type of solvent) appeared in all experiments after 15 days. On the contrary, VINPO-D-MAL and VINPO-DL-MAL never crystallised, and only gel-like products appeared on the bottom of the vials (Figures S1-S4 in the SI document). Fig. 2 reports the optical images of VINPO-L-MAL single crystals obtained in different solvents. The microscopic images showed that the single crystals obtained in EA were generally of the highest quality, thus they were used for single-crystal structure analysis.

Single crystal X-ray diffraction studies revealed that VINPO-L-MAL crystallises in the monoclinic space group $P2_1$ with one $VINPO^+$ cation and one $L\text{-}MAL^-$ anion in the asymmetric unit (Figure S5 in the SI document). The $L\text{-}MAL^-$ anions form two-dimensional molecular sheets *via* $O - H\bullet\bullet\bullet O^-$ hydrogen bonds. The $VINPO^+$ cations link to the molecular sheets through bifurcated $N^+ - H\bullet\bullet\bullet O^-/O$ hydrogen bonds (Fig. 3).

The thermal behaviour of VINPO-L-MAL (crystallised from EA) was subsequently investigated through DSC. The results are presented in Fig. 4 together with the DSC thermograms of the starting materials. Specifically, the DSC curve of the new system showed a single endothermic peak at 149.65 °C, with an enthalpy of 94.45 J g^{-1}, which was attributed to its melting. Interestingly, the melting point of VINPO-L-MAL single crystal is close to that of raw VINPO detected at 150.32 °C, while far from that of pure L-MAL that occurred at 103.52 °C. The DSC curves of other single crystals obtained in different solvents were comparable (Figure S6 in the SI document).

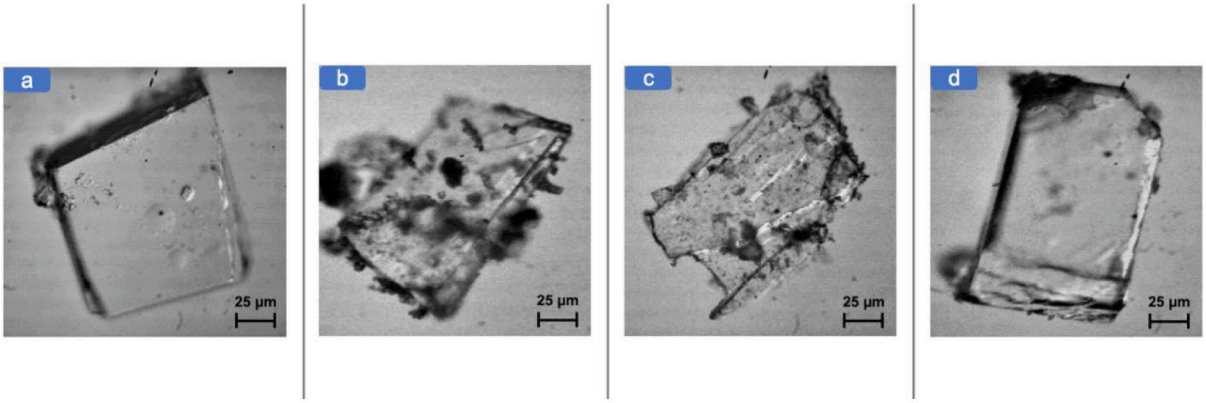

Fig. 2. Optical images of single crystals obtained in (a) EA, (b) EtOH, (c) AcT and (d) ACN at a magnification of 10x.

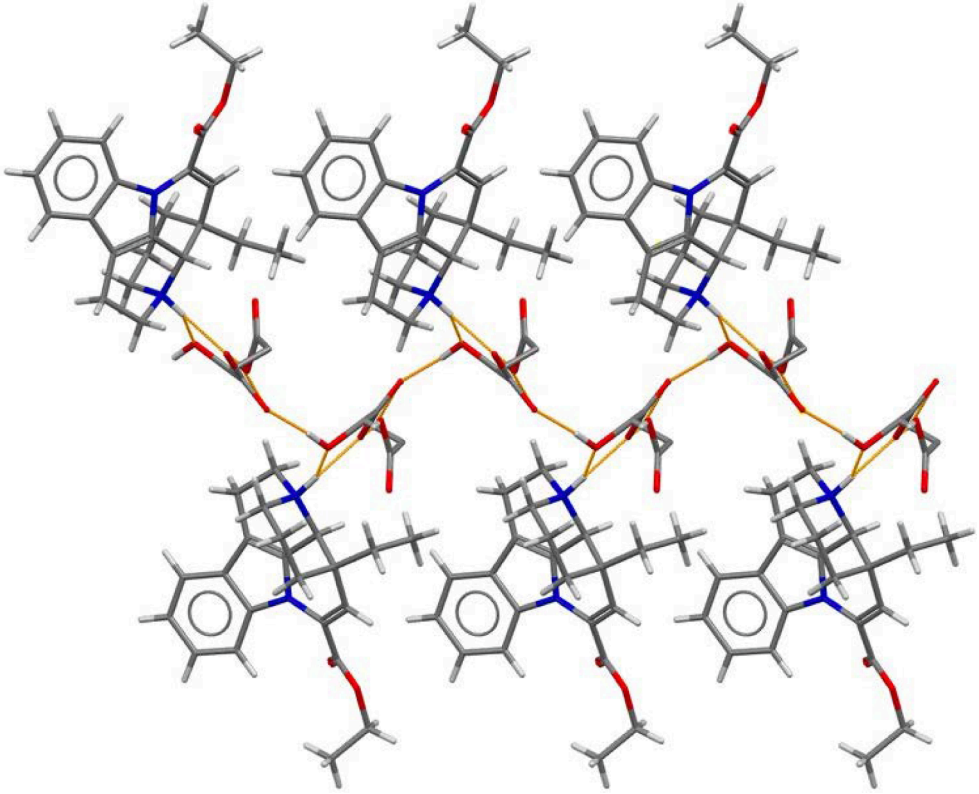

Fig. 3. $VINPO^{+}$: $L\text{-}MAL^{-}$ assemblies in the crystal structure of VINPO-L-MAL, as determined by single crystal X-ray diffraction analyses.

Hot-stage microscopy was also used for the *in-situ* observation of the samples upon heating. The results confirmed the DSC results: upon heating VINPO-L-MAL single crystals showed a unique thermal event corresponding to melting at about 149 °C (see the multimedia file in the SI document).

Mechanochemistry was subsequently used to understand if VINPO-L-MAL multicomponent crystalline system could also be obtained in the solid-state. As previously mentioned, different mechanochemical methods such as NG, LAG and POLAG were employed. The same techniques were also tested for VINPO-D-MAL and VINPO-DL-MAL.

NG led to the formation of an amorphous phase and traces of unreacted VINPO in all the three systems (Fig. 5). The literature has shown that NG can generate amorphous systems, while LAG, *i.e.* grinding in the presence of small amounts of catalytic liquids, usually brings to crystalline materials [36–38].

Interestingly, the amorphous solid consisting of VINPO-L-MAL obtained through NG (hereinafter VINPO-L-MAL-NG) spontaneously recrystallised after 2 months, while VINPO-D-MAL remained amorphous for the whole investigated period (48 months). VINPO-DL-MAL system showed a partial recrystallisation that was slower (12 months) than that observed in the enantiomerically-pure VINPO-L-MAL system (Figure S7 in the SI document). Additionally, DSC thermograms of the three samples confirmed the stability results: the thermogram of VINPO-L-MAL-NG showed a recrystallisation exothermic event at 122.15 °C followed by an endothermic event at 149.65 °C corresponding to the melting (Figure S8 in the SI document).

To better understand the above-mentioned physical stability results, the glass transition (T_g) values of the pure compounds and of the multicomponent systems were determined (see paragraph 2.2.2) and compared to the theoretical T_g*s* calculated by the Flory-Fox equation [39]. As reported in Table 1, melt quenched pure VINPO has a T_g of 22.31 °C, individual L-MAL or D-MAL enantiomers exhibit a T_g of

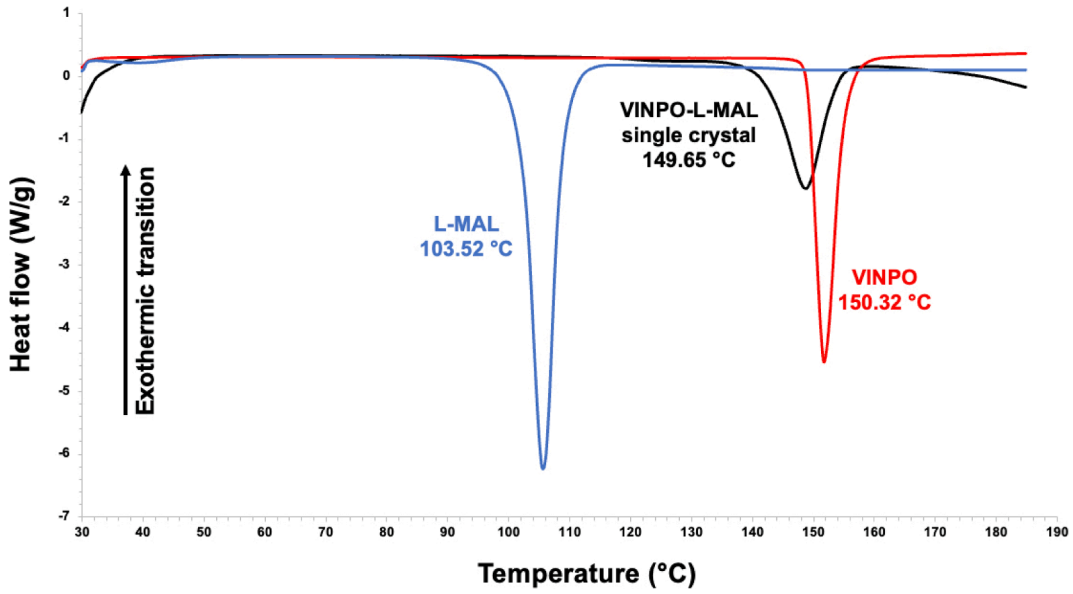

Fig. 4. DSC experimental curves of new VINPO-L-MAL multicomponent system (black), raw VINPO (red) and L-MAL (blue). (For interpretation of the references to colour in this figure legend, the reader is referred to the web version of this article.)

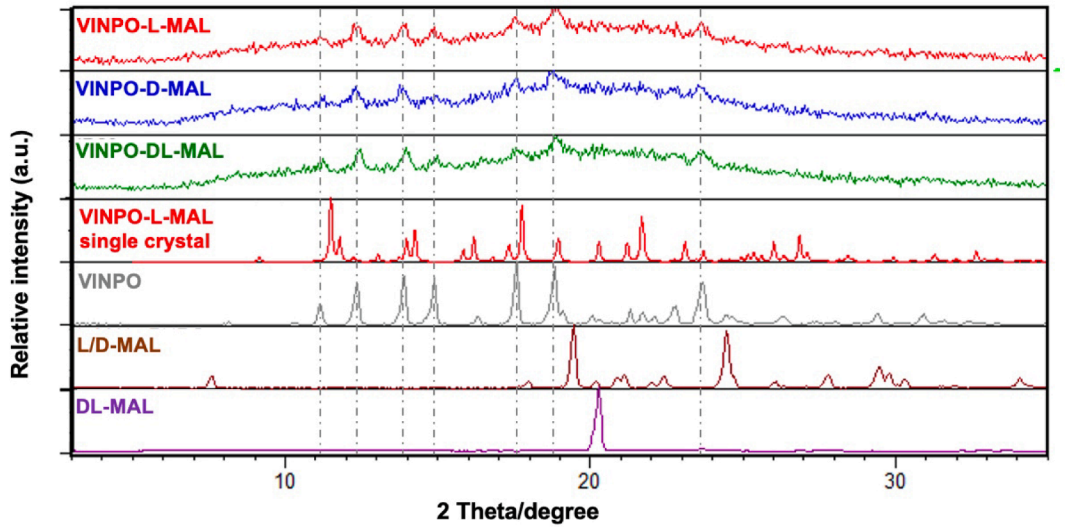

Fig. 5. PXRD patterns of NG mechanochemically prepared VINPO-L-MAL, VINPO-D-MAL, VINPO DL-MAL samples, plus VINPO-L-MAL single crystal and raw VINPO and MAL. Grey dotted lines highlight VINPO reflections.

Table 1
Experimental T_g values for raw materials and VINPO-L-MAL-NG, VINPO-D-MAL and VINPO-DL-MAL systems, compared (when possible) to the theoretical T_g according to the Flory-Fox equation.

Sample	Experimental T_g (°C)	Theoretical T_g according to Fox equation (°C)
VINPO	22.31	N/A[a]
L-MAL	−5.86	N/A[a]
D-MAL	−5.86	N/A[a]
DL-MAL	−13.11	N/A[a]
VINPO-L-MAL	59.92	13.93
VINPO-D-MAL	59.09	13.93
VINPO-DL-MAL	62.58	11.58

[a] Single compound, not applicable to calculate a theoretical T_g through the Flory-Fox equation [39].

−5.86 °C, while DL-MAL racemic compound a T_g of −13.11 °C, in accordance with the *Tg* values reported in literature [40]. T_g values of the three VINPO-MAL systems clearly differ from those of the pure compounds (Table 1). It is worth mentioning that the experimental T_g*s* of the multicomponent systems are not in accordance with the theoretical values, being the experimental T_g*s* approximately 30 °C higher than respective theoretical T_g*s* obtained through the Flory-Fox equation. Such differences were already reported for salt forming systems, that typically show significantly higher T_g values than the theoretical ones, attributable to the strong ionic interactions occurring in acid-base systems [41–44]. The experimental T_g*s* of the VINPO-L-MAL-NG and VINPO-D-MAL systems are identical. The different physical stability of the VINPO-L-MAL-NG and VINPO-D-MAL systems, therefore, cannot be related to the T_g values, but it rather depends on the enantiomer stereoselectivity. It is likely that only the L-enantiomer of MAL has the appropriate conformation to create a crystalline multicomponent solid with VINPO, while being the D-enantiomer not favourable from a steric

point of view for crystallisation, it forces the system towards an amorphous solid. Finally, the VINPO-DL-MAL system exhibits a slightly higher experimental T_g compared to those of VINPO-L-MAL and VINPO-D-MAL compounds, that can possibly explain the slower recrystallisation process (12 months) [45] than that observed for the enantiomerically-pure VINPO-L-MAL system (2 months).

In addition to NG, LAG experiments were also performed. The main aim of these experiments was to understand if it was possible to obtain a crystalline multicomponent system of VINPO in the presence of the other enantiomer D-MAL. The solvents were selected among those used for the solution crystallisations, with the addition of a non-polar liquid such as HXN (not previously used, since MAL is insoluble in such liquid).

As it is known from literature that for some multicomponent systems different amounts of the same liquid can lead to different polymorphs of the same system [20] or can promote the amorphization/crystallisation processes [21], in this case for each liquid, 4 different η values [24] ranging from a minimum of 0.1 to a maximum of 0.4 were used.

For the sake of brevity, in Fig. 6 PXRD results of LAG experiments with HXN are reported, while DSC results are presented in Figure S9 in the SI file.

As expected, LAG of VINPO-L-MAL in the presence of different amounts of HXN led to highly crystalline powdered solids (Fig. 6a). Similar results were obtained with all other liquids, and no evidence of different polymorphic forms of the new multicomponent system could be detected (Figure S10 in the SI file).

Interestingly, LAG of VINPO and D-MAL in the presence of HXN produced solids with a clear presence of unreacted VINPO (Fig. 6c). Although we did not perform quantitative analysis, it is evident from the PXRD pattern reported in Fig. 6c that the amount of unreacted VINPO increases at higher η values.

LAG experiments with VINPO and DL-MAL in the presence of different amounts of HXN led to the formation of solid products with different characteristics. Specifically, the solid obtained by LAG using an η value of 0.1 appeared mainly amorphous with traces of unreacted VINPO and it was very similar to the PXRD pattern of the VINPO-DL-MAL solid obtained by NG. At higher η values, a partially crystalline solid showing diffraction peaks corresponding to those of VINPO-L-MAL (plus some unreacted VINPO) were observed (Fig. 6b). It is likely that DL-MAL racemic compound, initially forms a conglomerate upon milling in the presence of enantiomerically pure VINPO. After that, VINPO separately interacts with each enantiomer forming a crystalline salt with the L-MAL enantiomer, and an amorphous salt with the opposite enantiomer.

A confirmation of this hypothesis was given by another LAG experiment (1 h of LAG HXN at 25 Hz) in which VINPO was milled in the presence of a physical mixture of L-MAL and D-MAL (hereinafter referred to as VINPO-D-L-MAL PM). VINPO-D-L-MAL PM – through PXRD characterization – showed a partially crystalline pattern perfectly superimposable to that of VINPO-DL-MAL, presenting diffraction peaks corresponding to those of VINPO-L-MAL plus signals due to unreacted VINPO. Since grinding VINPO in the presence of DL-MAL as racemic compound or as physical mixture gave the same result, we could strongly support the thesis that a transition from DL-MAL racemic compound to a conglomerate occurs upon LAG in the presence of enantiomerically pure VINPO, allowing VINPO to separately interact with each enantiomer, finally coming to the preferential crystallization with the L-MAL enantiomer. Figure S11 in the SI document shows a PXRD comparison of VINPO-D-L-MAL PM and VINPO-DL-MAL.

A summary of all LAG results is reported in Table S3 in the SI file. Generally, when VINPO is processed in the presence of L-MAL, a new crystalline product is consistently produced, regardless of the type and amount of liquid used. When VINPO is processed in the presence of D-MAL a completely different scenario appears: the material appeared deliquescent immediately after the LAG process finished (with all liquids, except for HXN) (Fig. 7).

The mechanochemical formation of deliquescent materials is not new and has been observed even when no intentional water is added into the milling jar, but simply due to the humidity in the air [46]. Clearly, such phenomenon depends on the experimental conditions and on the propensity of specific multicomponent systems of being hygroscopic [47]. However, the formation of deliquescent materials in the case of VINPO-D-MAL system cannot be related to the humidity since NG of the system produced a free-flowing amorphous solid, but such phenomenon became particularly evident when liquids with a certain polarity (including low polar liquids such as EA) were added [48].

Additionally, POLAG experiments of VINPO-D-MAL also produced free-flowing (yet amorphous) solids (see Figures S13 and S14 in the SI document), and we have previously observed that specific polymers can dehydrate hydrated solids [49,50]. It is therefore reasonable to think that the deliquescence observed in the case of VINPO-D-MAL can be related, due to the amorphous nature of the system, to a possible partial absorption or interaction with the molecules of the added liquid.

The behaviour of the system consisting of VINPO and DL-MAL was in between the two enantiomerically pure systems; only with HXN, free-flowing products were obtained, being amorphous at low η values and producing a partially crystalline solid with diffraction peaks corresponding to the VINPO-L-MAL system at higher η values (see Fig. 6). LAG experiments with the other tested liquids on VINPO-DL-MAL always gave a deliquescent material (see Figure S14 in the SI document).

Subsequently, SSNMR analyses were performed to confirm the

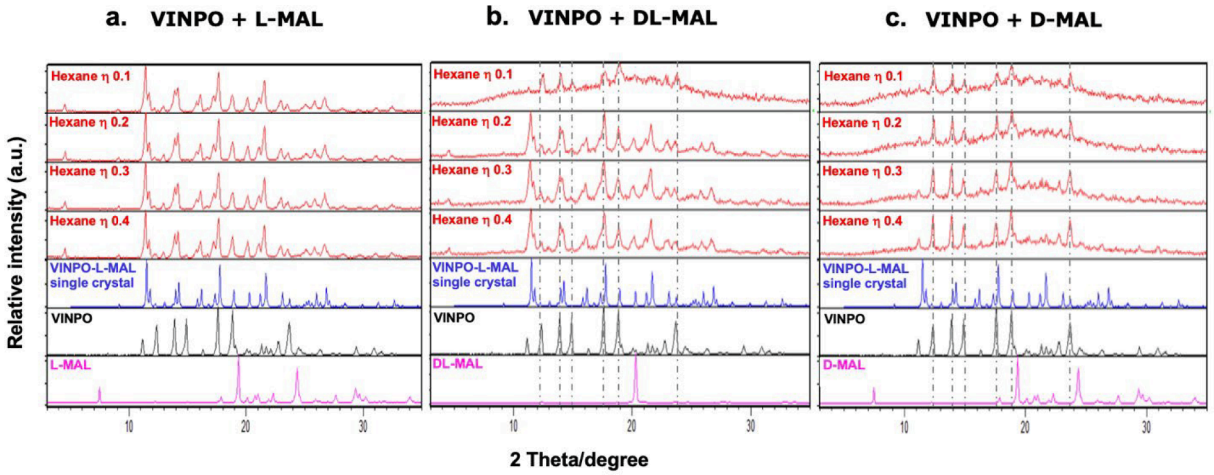

Fig. 6. PXRD results of LAG experiments with 0.1, 0.2, 0.3, 0.4 η of HXN for (a) VINPO-L-MAL, (b) VINPO-DL-MAL and (c) VINPO-D-MAL three systems. Grey dotted lines highlight VINPO reflections.

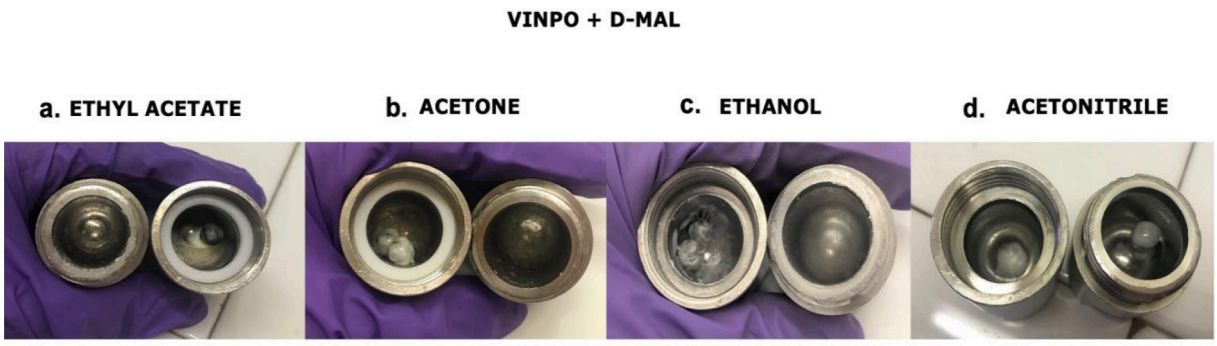

Fig. 7. Images of opened jars showing VINPO-D-MAL deliquescent material after LAG experiments with (a) EA, (b) AcT, (c) EtOH and (d) ACN.

protonation state of VINPO in the different VINPO-MAL systems, *i.e.*, the formation of salts or cocrystals. From literature it is well-known that the empirical ΔpK_a rule (pK_a (protonated base) − pK_a (acid)) can be generally used for predicting salt from cocrystal formation. According to such rule, when the ΔpK_a is greater than 3, a complete proton transfer occurs leading to a salt, while when lower than −1 often brings to the formation of neutral cocrystal system [51,52]. On the other hand, between −1 and 3 the prediction is no longer possible [53]. However, although the predictive accuracy of the pK_a is generally high, the protonation state must be always supported by experimental spectroscopic data [54].

In the case of VINPO and MAL, they interact with each other via a N···H···O contact between N11 of VINPO and a carboxylic group of MAL, as observed in the crystal structure and for similar systems [34,35]. For such interaction, the ΔpK_a is equal to 3.80 (pK_a (protonated VINPO) 7.31 – pK_{a1}(MAL) 3.51) [55,56], suggesting a higher probability of obtaining molecular salts, *i.e.* characterized by ionic interactions between the two molecules.

The ^{13}C CPMAS spectrum recorded for VINPO-L-MAL is shown in Fig. 8a, where it is compared with those of pure VINPO and L-MAL. In the VINPO-L-MAL spectrum, only one set of resonances appears for both VINPO and L-MAL, at different chemical shift than in the starting materials, confirming that a new crystal form with a 1:1 stoichiometry is obtained. Importantly, VINPO-L-MAL does not contain detectable traces of unreacted starting materials. It is widely recognised that a comparison of the chemical shifts of the carboxyl groups of the pure coformer with the same signals of the multicomponent systems could provide information on the protonation state of the API, *i.e.* whether the hydrogen bond interaction is assisted by a proton transfer from the carboxyl group of the coformer to the basic N11 of the VINPO [52]. In these particular case, the shifts with respect to pure L-MAL are not very indicative for two reasons: a) pure L-MAL contains two independent molecules in the unit cell, as evinced by the splitting of almost all peaks (CSD identifier: COFRUK10), thus it is not easy to correlate the shifts to the correct signals; b) in pure L-MAL all (4) carboxylic groups are involved in COOH-HOOC homosynthons to form the $R_2^2(8)$ motif which is well known to shift the COOH signal at higher frequencies similar to that of carboxylate groups [57]. However, the carboxylic carbon C1′ and C4′ signals resonate at 173.6 and 180.1 ppm and their difference in chemical shift suggests the presence of two carboxylic groups having different protonation state: a carboxylic acid (173.6 ppm) and a carboxylate (180.1 ppm), in agreement with shift values reported in literature [52].

Fig. 8b displays an analogous comparison between the ^{15}N CPMAS spectra of VINPO-L-MAL and pure VINPO. The presence of only two signals in the spectrum of the new system confirms the 1:1 stoichiometry surmised by the ^{13}C CPMAS spectrum. Moreover, the shift of the N11 signal at higher frequencies, from 29.3 ppm in pure VINPO to 42.9 ppm in VINPO-L-MAL ($\Delta\delta = 13.6$ ppm), is such to justify its protonation with formation of a charge-assisted N^+-H···O^- interaction with the carboxylic group of L-MAL. Similar shifts were observed in the case of salts VINPO-boric acid, VINPO-citrate and VINPO-oxalic acid [26,34].

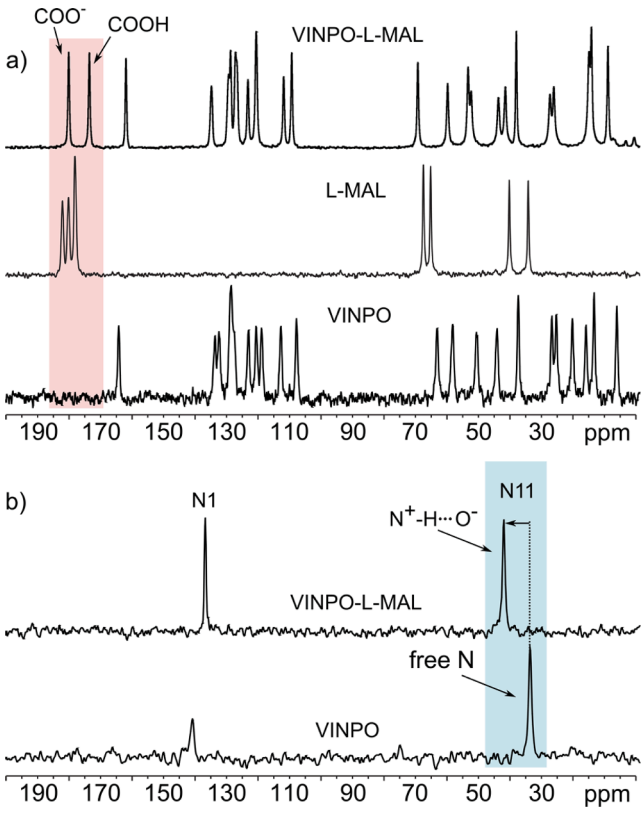

Fig. 8. (a) ^{13}C (100.6 MHz) CPMAS spectra of VINPO-L-MAL, pure L-MAL and pure VINPO acquired at a spinning speed of 12 kHz at room temperature. The red box highlights signals related to L-MAL carboxylic carbons. (b) ^{15}N (40.6 MHz) CPMAS spectra of VINPO-L-MAL and pure VINPO acquired at a spinning speed of 9 kHz at room temperature. The blue box highlights signals related to the VINPO N11 atom. (For interpretation of the references to colour in this figure legend, the reader is referred to the web version of this article.)

A comparison among ^{13}C CPMAS spectra of crystalline VINPO-L-MAL, VINPO-L-MAL-NG and VINPO-D-MAL is presented in Fig. 9. The signals in the spectra exhibit an average full width at half maximum value of ~ 70 Hz for crystalline VINPO-L-MAL, ~330 Hz for VINPO-L-MAL-NG and ~ 280 Hz for VINPO-D-MAL. These values agree with the crystalline and amorphous nature of the three analysed powders. It is important to highlight the presence of traces of unreacted VINPO in VINPO-L-MAL-NG and VINPO-D-MAL, mainly observable in the shoulders at 21.4, 59.4, 64.6 and 164.3 ppm. On the other hand, no signals of unreacted D-MAL are observed in VINPO-D-MAL (see Figure S15 in the SI document).

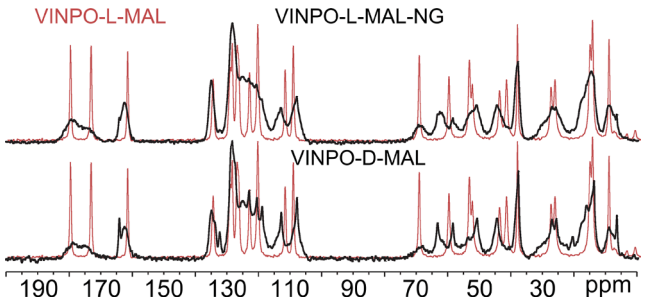

Fig. 9. ^{13}C (100.6 MHz) CPMAS spectra of crystalline VINPO-L-MAL (red), VINPO-L-MAL-NG (black, up) and VINPO-D-MAL (black, down) acquired at a spinning speed of 12 kHz at room temperature. (For interpretation of the references to colour in this figure legend, the reader is referred to the web version of this article.)

The considerations drawn for VINPO-L-MAL regarding the carboxylic and N11 protonation state are also valid for VINPO-L-MAL-NG, although the signals are much broader in accordance with the synthetic technique used for the sample preparation. The ^{13}C (Fig. 9) and ^{15}N CPMAS (Figure S16 in the SI document) spectra mostly reproduce very similar chemical shifts for the resonances associated to C1′, C4′ and N11 with respect to the crystalline VINPO-L-MAL. Indeed, the ^{13}C C1′ and C4′ peaks are centred at about 179.0 and 174.4 ppm ascribable to a COO^- and a COOH environments, respectively, while the ^{15}N N11 signal falls at 44.6 ppm typical of a N^+-H group. The same applies for VINPO-D-MAL, which has carboxyl signals very similar to VINPO-L-MAL-NG (Fig. 9) (178.9 and 175.3 ppm) but whose ^{15}N CPMAS spectrum was not acquired because of the presence of a large amount of unreacted VINPO. The broadening and the presence of additional signals in the spectra reveal the amorphousness of these samples and a transition towards the formation of a new, but not complete and pure, multicomponent form.

Finally, Fig. 10 shows the ^{13}C CPMAS spectra of VINPO-DL-MAL (synthetised by LAG using HXN as liquid with a η value of 0.4) compared to pure VINPO and VINPO-L-MAL. The signal in VINPO-DL-MAL exhibits an average full width half maximum value of ~ 100 Hz; this confirms the crystalline nature of the sample, previously detected by PXRD. Furthermore, from the ^{13}C CPMAS spectra, it is possible to clearly recognise the same crystalline form as VINPO-L-MAL. Indeed, most of the chemical shift values of the signals are perfectly superposable with those of VINPO-L-MAL. However, a significant amount of unreacted VINPO is present, as observed from the signals at 7.5, 51.2, 58.6, 63.8, 108.0, 119.2, 132.5 and 164.2 ppm. The unreacted VINPO was estimated to be approximately 20–25 %, by integration of relevant signals, and highlights the inability of the system to completely convert to a new pure crystalline form in the presence of the D-MAL enantiomer. This confirms the hypothesis of a preferential and selective crystallisation of VINPO with the L-MAL enantiomer. On the other hand, no signals of unreacted D- nor DL-MAL are observed (see Figure S17 in the SI document).

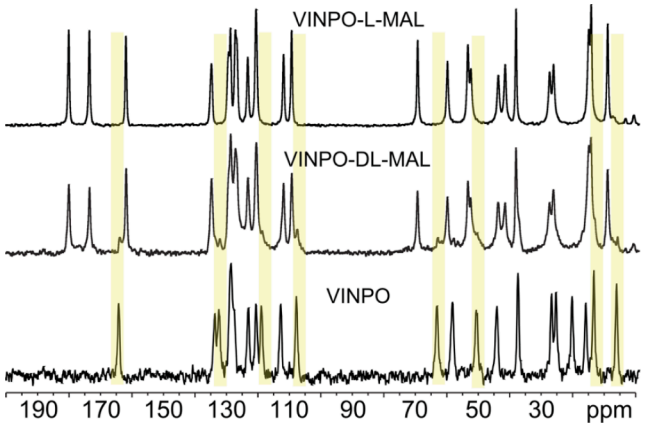

Fig. 10. ^{13}C (100 MHz) CPMAS spectra of VINPO-DL-MAL system, compared to pure VINPO and crystalline VINPO-L-MAL acquired at a spinning speed of 12 kHz at room temperature. Yellow boxes highlight VINPO signals present in VINPO-DL-MAL. (For interpretation of the references to colour in this figure legend, the reader is referred to the web version of this article.)

Finally, the dissolution kinetic tests for the crystalline VINPO-L-MAL, VINPO-D-MAL and partially crystalline VINPO-DL-MAL salts were carried out at 37 °C in a pH 7.4 phosphate buffer. As it is evident from Fig. 11, all three above-mentioned systems showed a remarkable improvement of the dissolving performance when compared to raw VINPO. The dissolution profile of the three products is typical of a salt, that is a rapid solubilisation reaching large supersaturation within the first 2 min of the test, followed by a precipitation phase. In all three products the concentration reaches a plateau value of about 2 mg L^{-1} within the first 30 min of testing, which is in accordance with the equilibrium solubility, reported in the literature [35]. However, it is worth noticing that the dissolution profile of VINPO-L-MAL salt is higher, both in terms of maximum concentration reached and extent of the spring-parachute phenomenon [58–60], compared to those of VINPO-D-MAL and partially crystalline VINPO-DL-MAL salts, which is in contradiction with what is commonly known from literature [51,61,62]. Indeed, the mean area under the curve (AUC) for VINPO-L-MAL is 500.0 ± 14.1 mg L^{-1}, while the mean AUC values for VINPO-D-MAL and VINPO-DL-MAL are 265.0 ± 34.7 and 307.8 ± 9.9, respectively (Table 2).

A possible explanation of this phenomenon can be related to the fact that only the crystalline VINPO-L-MAL salt is a pure system with no traces of unreacted VINPO, while both VINPO-D-MAL and VINPO-DL-MAL systems present residues of unreacted VINPO, as attested by PXRD and SSNMR analyses. The presence of traces of the poorly soluble drug VINPO can affect the degree of solubilisation in these two systems, having therefore a significant impact on their dissolution profile. Potentially, the presence of suspended unreacted VINPO crystals can also accelerate the precipitation phenomenon, by acting as pre-formed seeds on which VINPO molecules precipitate from the solution and attach on their surface. This result highlights the fact that the physical status (amorphous or crystalline) but also the phase purity is an important factor necessary to better understand the dissolution behaviour of new solid forms.

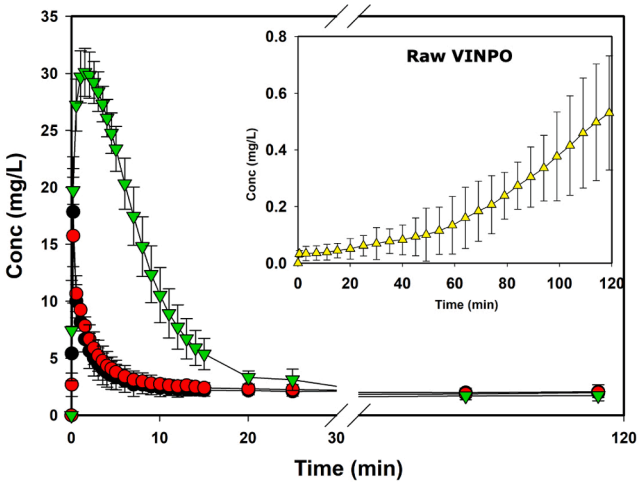

Fig. 11. Dissolution profiles of pure VINPO (yellow triangles) compared to crystalline VINPO-L-MAL (green triangles), VINPO-D-MAL (red circles) and partially crystalline VINPO-DL-MAL (black circles). (For interpretation of the references to colour in this figure legend, the reader is referred to the web version of this article.)

Table 2
Mean area under the curve (AUC) for VINPO-L-MAL, VINPO-D-MAL, VINPO-DL-MAL systems and raw VINPO.

Sample	Mean AUC ((mg L^{-1} min) ± S.D.
VINPO	23.6 ± 9.3
VINPO-L-MAL	500.0 ± 14.1
VINPO-D-MAL	265.0 ± 34.7
VINPO-DL-MAL	307.8 ± 9.9

4. Conclusions

The crystallisation tendency of VINPO in the presence of individual enantiomers and racemic form of MAL was investigated both in solution crystallisations and through mechanochemistry. Despite several techniques, VINPO presented a preferential crystallization tendency with L-MAL, while experiments with D-MAL consistently generated amorphous and deliquescent materials. The new VINPO-L-MAL system crystallizes in the monoclinic $P2_1$ space group, showing one VINPO and one L-MAL molecule in the asymmetric unit.

While ^{13}C and ^{15}N CPMAS SSNMR experiments confirmed the protonation state of VINPO in all three systems, only VINPO-L-MAL appeared a pure phase, while the VINPO-D-MAL amorphous salt still presented residual peaks of unreacted VINPO. The VINPO-DL-MAL system was partially crystalline (with also traces of unreacted VINPO) with diffraction peaks corresponding to those of VINPO-L-MAL. An explanation of this phenomenon could be found in a possible conversion of the racemic compound to a conglomerate during milling, which subsequently allows VINPO to separately interact with each MAL enantiomer, preferentially crystallizing with L-MAL, while giving an amorphous solid with D-MAL.

Finally, dissolution tests were performed on the three VINPO-L-MAL, VINPO-D-MAL and VINPO-DL-MAL systems, to check whether an improvement of pure VINPO dissolution profile could occur: all the three systems showed a significant improvement of the dissolving performance when compared to raw VINPO. It is noteworthy that the dissolution profile of crystalline VINPO-L-MAL salt is superior compared to those of VINPO-D-MAL and partially crystalline VINPO-DL-MAL salts, presumably due to the presence of significant traces of the poorly soluble drug VINPO which could greatly decrease the solubility values of VINPO-D-MAL and VINPO-DL-MAL systems.

The system investigated in this study represents an interesting example of how chirality can significantly affect the solid-state properties of a compound, including the propensity to form a pure crystalline or amorphous system, with potential consequences both in the solid-state properties/stability and biopharmaceutical characteristics.

CRediT authorship contribution statement

Ilenia D'Abbrunzo: Writing – review & editing, Writing – original draft, Methodology, Formal analysis, Data curation. **Rebecca Birolo:** Review & editing, Writing NMR comments, Methodology, Investigation. **Michele R. Chierotti:** Writing – review & editing, Validation, Methodology, Investigation. **Dejan-Krešimir Bučar:** Writing – review & editing, Resources, Methodology, Investigation, Data curation. **Dario Voinovich:** Writing – review & editing, Supervision, Methodology, Investigation, Data curation. **Beatrice Perissutti:** Writing – review & editing, Writing – original draft, Supervision, Investigation, Formal analysis, Data curation. **Dritan Hasa:** Writing – review & editing, Writing – original draft, Visualization, Supervision, Project administration, Conceptualization.

Declaration of competing interest

The authors declare that they have no known competing financial interests or personal relationships that could have appeared to influence the work reported in this paper.

Data availability

A Supplementary Information file, the CIF and other information are available

Acknowledgements

M.R.C. and R.B. acknowledge support from the Project CH4.0 under the MUR program "Dipartimenti di Eccellenza 2023-2027" (CUP: D13C22003520001). DH and ID would thank Prof. Tomislav Friscic (University of Birmingham) for useful discussions.

Appendix A. Supplementary data

Supplementary data to this article can be found online at https://doi.org/10.1016/j.ejpb.2024.114344.

References

[1] C. Viedma, G. Coquerel, P. Cintas, Crystallization of Chiral Molecules, in: Handbook of Crystal Growth, Elsevier, 2015: pp. 951–1002. 10.1016/B978-0-444-56369-9.00022-8.
[2] R. Kaviani, A. Jouyban, A. Shayanfar, Chiral resolution methods for racemic pharmaceuticals based on cocrystal formation, CrstEngComm 25 (2023) 6120–6131, https://doi.org/10.1039/D3CE00853C.
[3] F.-D. Lung, J.-P. Meyer, G. Li, B.-S. Lou, D. Stropova, P. Davis, H.I. Yamamura, F. Porreca, V.J. Hruby, Highly kappa receptor-selective dynorphin A analogues with modifications in position 3 of dynorphin A(1–11)-NH2, J Med Chem 38 (1995) 585–586, https://doi.org/10.1021/jm00004a002.
[4] J. Markwell, Molecules and medicine by E.J. Corey, B Czakó, and L. Kürti, Biochem. Mol. Biol. Educ. 36 (2008) 245–246, https://doi.org/10.1002/bmb.20179.
[5] H. Rouh, Y. Tang, T. Xu, Q. Yuan, S. Zhang, J.-Y. Wang, S. Jin, Y. Wang, J. Pan, H. L. Wood, J.D. McDonald, G. Li, Aggregation-induced synthesis (AIS): asymmetric synthesis via chiral aggregates, Research 2022 (2022), https://doi.org/10.34133/2022/9865108.
[6] N. Ananthi, Role of chirality in drugs, OMCIJ 5 (2018), https://doi.org/10.19080/OMCIJ.2018.05.555661.
[7] W. Li, M. de Groen, H.J.M. Kramer, R. de Gelder, P. Tinnemans, H. Meekes, J.H. ter Horst, Screening approach for identifying cocrystal types and resolution opportunities in complex chiral multicomponent systems, Cryst. Growth Des. 21 (2020) 112–124, https://doi.org/10.1021/acs.cgd.0c00890.
[8] J. Sun, Y. Wang, W. Tang, J. Gong, Enantioselectivity of chiral dihydromyricetin in multicomponent solid solutions regulated by subtle structural mutation, IUCrJ 10 (2023) 164–176, https://doi.org/10.1107/S2052252523000118.
[9] C.J.J. Gerard, C. Pinetre, H. Cercel, M.D. Charpentier, M. Sanselme, N. Couvrat, C. Brandel, Y. Cartigny, V. Dupray, J.H. Ter Horst, Phase diagrams of praziquantel and vanillic acid cocrystals: racemic compound and conglomerate system, Cryst. Growth Des. 24 (2024) 3378–3387, https://doi.org/10.1021/acs.cgd.4c00114.
[10] L. Wang, N. Wang, J. Sui, S. Sun, Z. Feng, G. Li, H. Hao, L. Zhou, Case of chiral resolution through converting two racemic compounds into a conglomerate, Cryst. Growth Des. 23 (2023) 5641–5650, https://doi.org/10.1021/acs.cgd.3c00311.
[11] L. Song, O. Shemchuk, K. Robeyns, D. Braga, F. Grepioni, T. Leyssens, Ionic cocrystals of etiracetam and levetiracetam: the importance of chirality for ionic cocrystals, Cryst. Growth Des. 19 (2019) 2446–2454, https://doi.org/10.1021/acs.cgd.9b00136.
[12] T. Rekis, Crystallization of chiral molecular compounds: what can be learned from the Cambridge Structural Database? Acta Crystallogr B Struct Sci Cryst Eng Mater 76 (2020) 307–315, https://doi.org/10.1107/S2052520620003601.
[13] E. Grothe, H. Meekes, R. de Gelder, Chirality and stereoisomerism of organic multicomponent crystals in the CSD, CrstEngComm 22 (2020) 7380–7388, https://doi.org/10.1039/D0CE00403K.
[14] G. Springuel, K. Robeyns, B. Norberg, J. Wouters, T. Leyssens, Cocrystal formation between chiral compounds: how cocrystals differ from salts, Cryst. Growth Des. 14 (2014) 3996–4004, https://doi.org/10.1021/cg500588t.
[15] Vinpocetine, European Pharmacopoeia Ph. Eur. 11th Ed. (2008) 2139.
[16] D. Hasa, B. Perissutti, S. Dall'Acqua, M.R. Chierotti, R. Gobetto, I. Grabnar, C. Cepek, D. Voinovich, Rationale of using Vinca minor Linne dry extract phytocomplex as a vincamine's oral bioavailability enhancer, Eur J Pharm Biopharm 84 (2013) 138–144, https://doi.org/10.1016/j.ejpb.2012.11.025.
[17] L.S.S. Ribeiro, A.C. Falcão, J.A.B. Patrício, D.C. Ferreira, F.J.B. Veiga, Cyclodextrin multicomponent complexation and controlled release delivery strategies to optimize the oral bioavailability of vinpocetine, J Pharm Sci 96 (2007) 2018–2028, https://doi.org/10.1002/JPS.20294.

[18] Y. Shuai Zhang, J. Dong Li, C. Yan, An update on vinpocetine: New discoveries and clinical implications, Eur J Pharmacol 819 (2018) 30–34, https://doi.org/10.1016/j.ejphar.2017.11.041.
[19] P. Bönöczk, B. Gulyás, V. Adam-Vizi, A. Nemes, E. Kárpáti, B. Kiss, M. Kapás, C. Szántay, I. Koncz, T. Zelles, A. Vas, Role of sodium channel inhibition in neuroprotection: effect of vinpocetine, Brain Res Bull 53 (2000) 245–254, https://doi.org/10.1016/S0361-9230(00)00354-3.
[20] A.J. Cruz-Cabeza, M. Lestari, M. Lusi, Cocrystals help break the "rules" of isostructurality: solid solutions and polymorphism in the malic/tartaric acid system, Cryst. Growth Des. 18 (2017) 855–863, https://doi.org/10.1021/acs.cgd.7b01321.
[21] P.J. Sheskey, B.C. Hancock, G.P. Moss, D.J. Goldfarb, Handbook of pharmaceutical excipients, Ninth edition, Pharmaceutical Press, London, 2020.
[22] C. Marques, A.R. Sotiles, F. Oliveira Farias, G. Oliveira, M. Leite, M.-D. Daltoé c, M. L. Masson, Full physicochemical characterization of malic acid: Emphasis in the potential as food ingredient and application in pectin gels Production and hosting by Elsevier, (2020). 10.1016/j.arabjc.2020.10.036.
[23] D. Hasa, W. Jones, Screening for new pharmaceutical solid forms using mechanochemistry: A practical guide, Adv Drug Deliv Rev. 117 (2017) 147–161, https://doi.org/10.1016/j.addr.2017.05.001.
[24] T. Friščić, S.L. Childs, S.A.A. Rizvi, W. Jones, The role of solvent in mechanochemical and sonochemical cocrystal formation: a solubility-based approach for predicting cocrystallisation outcome, CrstEngComm 11 (2009) 418–426, https://doi.org/10.1039/B815174A.
[25] D. Hasa, E. Miniussi, W. Jones, Mechanochemical synthesis of multicomponent crystals: one liquid for one polymorph? A Myth to Dispel, Cryst Growth Des 16 (2016) 4582–4588, https://doi.org/10.1021/acs.cgd.6b00682.
[26] M. Arhangelskis, D.-K. Bučar, S. Bordignon, M.R. Chierotti, S.A. Stratford, D. Voinovich, W. Jones, D. Hasa, Mechanochemical reactivity inhibited, prohibited and reversed by liquid additives: examples from crystal-form screens, Chem Sci 12 (2021) 3264–3269, https://doi.org/10.1039/D0SC05071G.
[27] D. Hasa, G. Schneider Rauber, D. Voinovich, W. Jones, Cocrystal formation through mechanochemistry: from neat and liquid-assisted grinding to polymer-assisted grinding, Angew Chem Int Ed 54 (2015) 7371–7375, https://doi.org/10.1002/anie.201501638.
[28] L.S. Germann, S.T. Emmerling, M. Wilke, R.E. Dinnebier, M. Moneghini, D. Hasa, Monitoring polymer-assisted mechanochemical cocrystallisation through in situ X-ray powder diffraction, ChemComm 56 (2020) 8743–8746, https://doi.org/10.1039/D0CC03460F.
[29] *CrysAlisPro, Agilent Technologies Inc.*, (2022).
[30] G.M. Sheldrick, SHELXT - Integrated space-group and crystal-structure determination, Acta Crystallogr A 71 (2015) 3–8, https://doi.org/10.1107/S2053273314026370.
[31] O.V. Dolomanov, L.J. Bourhis, R.J. Gildea, J.A.K. Howard, H. Puschmann, OLEX2: a complete structure solution, refinement and analysis program, J. Appl. Cryst. 42 (2009) 339–341, https://doi.org/10.1107/S0021889808042726.
[32] G.M. Sheldrick, Crystal structure refinement with SHELXL, Acta Crystallogr C Struct Chem 71 (2015) 3–8, https://doi.org/10.1107/S2053229614024218.
[33] C.B. Hübschle, G.M. Sheldrick, B. Dittrich, ShelXle: a Qt graphical user interface for SHELXL, J. Appl. Cryst. 44 (2011) 1281–1284, https://doi.org/10.1107/S0021889811043202.
[34] S. Golob, M. Perry, M. Lusi, M.R. Chierotti, I. Grabnar, L. Lassiani, D. Voinovich, M. J. Zaworotko, Improving biopharmaceutical properties of vinpocetine through cocrystallization, J Pharm Sci 105 (2016) 3626–3633, https://doi.org/10.1016/j.xphs.2016.09.017.
[35] D. Hasa, D. Voinovich, B. Perissutti, M. Grassi, A. Bonifacio, V. Sergo, C. Cepek, M. R. Chierotti, R. Gobetto, S. Dall'Acqua, S. Invernizzi, Enhanced oral bioavailability of vinpocetine through mechanochemical salt formation: physico-chemical characterization and in vivo studies, Pharm Res 28 (2011) 1870–1883, https://doi.org/10.1007/s11095-011-0415-8.
[36] S. Karki, T. Friscic, W. Jones, W.D.S. Motherwel, Screening for Pharmaceutical Cocrystal Hydrates via Neat and Liquid-Assisted Grinding, Mol. Pharmaceutics 4 (2007) 347–357, https://doi.org/10.1021/mp0700054.
[37] L. Gonnet, T.H. Borchers, C.B. Lennox, J. Vainauskas, Y. Teoh, H.M. Titi, C. J. Barrett, S.G. Koenig, K. Nagapudi, T. Friščić, The "η-sweet-spot" (ηmax) in liquid-assisted mechanochemistry: polymorph control and the role of a liquid additive as either a catalyst or an inhibitor in resonant acoustic mixing (RAM), Faraday Discuss 241 (2023) 128–149, https://doi.org/10.1039/D2FD00131D.
[38] K.K. Sarmah, N. Nath, D.R. Rao, R. Thakuria, Mechanochemical synthesis of drug–drug and drug–nutraceutical multicomponent solids of olanzapine, CrstEngComm 22 (2020) 1120–1130, https://doi.org/10.1039/C9CE01504C.
[39] P.J. Skrdla, P.D. Floyd, P.C. Dell'Orco, The amorphous state: first-principles derivation of the Gordon-Taylor equation for direct prediction of the glass transition temperature of mixtures; estimation of the crossover temperature of fragile glass formers; physical basis of the "Rule of 2/3", Phys. Chem. Chem. Phys. 19 (2017) 20523–20532, https://doi.org/10.1039/C7CP04124A.
[40] H. Hou, Q. Chen, J. Bi, B. Bhandari, X. Wu, X. Jin, Y. Shi, Y. Qiao, M. Gou, J. Shi, Glass transition and crystallization of solid model system of jujube slice as influenced by sugars and organic acids, Food Chem 359 (2021) 129935, https://doi.org/10.1016/j.foodchem.2021.129935.
[41] K. Löbmann, R. Laitinen, C. Strachan, T. Rades, H. Grohganz, Amino acids as co-amorphous stabilizers for poorly water-soluble drugs – Part 2: Molecular interactions, Eur J Pharm Biopharm 85 (2013) 882–888, https://doi.org/10.1016/J.EJPB.2013.03.026.
[42] W. Wu, K. Löbmann, T. Rades, H. Grohganz, On the role of salt formation and structural similarity of co-formers in co-amorphous drug delivery systems, Int J Pharm 535 (2018) 86–94, https://doi.org/10.1016/J.IJPHARM.2017.10.057.
[43] K.-I. Izutsu, S. Kadoya, C. Yomota, T. Kawanishi, E. Yonemochi, K. Terada, Freeze-drying of proteins in glass solids formed by basic amino acids and dicarboxylic acids, Chem Pharm Bull 57 (2009) 43–48, https://doi.org/10.1248/cpb.57.43.
[44] H. Ueda, W. Wu, K. Löbmann, H. Grohganz, A. Müllertz, T. Rades, Application of a salt coformer in a co-amorphous drug system dramatically enhances the glass transition temperature: a case study of the ternary system carbamazepine, citric acid, and l-arginine, Mol Pharm 15 (2018) 2036–2044, https://doi.org/10.1021/acs.molpharmaceut.8b00174.
[45] J. Buitink, I.J. van den Dries, F.A. Hoekstra, M. Alberda, M.A. Hemminga, High critical temperature above Tg may contribute to the stability of biological systems, Biophys J 79 (2000) 1119–1128, https://doi.org/10.1016/S0006-3495(00)76365-X.
[46] I.A. Tumanov, A.A.L. Michalchuk, A.A. Politov, E.V. Boldyreva, V.V. Boldyrev, Inadvertent liquid assisted grinding: a key to "dry" organic mechano-co-crystallisation? CrstEngComm 19 (2017) 2830–2835, https://doi.org/10.1039/C7CE00517B.
[47] T.S. Thakur, R. Thakuria, Crystalline multicomponent solids: an alternative for addressing the hygroscopicity issue in pharmaceutical materials, Cryst. Growth Des. 20 (2020) 6245–6265, https://doi.org/10.1021/acs.cgd.0c00654.
[48] K.K. Sarmah, T. Rajbongshi, A. Bhuyan, R. Thakuria, Effect of solvent polarity in mechanochemistry: preparation of a conglomerate vs racemate, ChemComm 55 (2019) 10900–10903, https://doi.org/10.1039/C9CC05687D.
[49] D. Scaramuzza, G. Schneider Rauber, D. Voinovich, D. Hasa, Dehydration without heating: use of polymer-assisted grinding for understanding the stability of hydrates in the presence of polymeric excipients, Cryst. Growth Des. 18 (2018) 5245–5253, https://doi.org/10.1021/acs.cgd.8b00687.
[50] M.W. Terban, L. Madhau, A.J. Cruz-Cabeza, P.O. Okeyo, M. Etter, A. Schulz, J. Rantanen, R.E. Dinnebier, S.J.L. Billinge, M. Moneghini, D. Hasa, Controlling desolvation through polymer-assisted grinding, CrstEngComm 24 (2022) 2305–2313, https://doi.org/10.1039/D2CE00162D.
[51] D.J. Berry, J.W. Steed, Pharmaceutical cocrystals, salts and multicomponent systems; intermolecular interactions and property-based design, Adv Drug Deliv Rev. 117 (2017) 3–24, https://doi.org/10.1016/j.addr.2017.03.003.
[52] P. Cerreia Vioglio, M.R. Chierotti, R. Gobetto, Pharmaceutical aspects of salt and cocrystal forms of APIs and characterization challenges, Adv Drug Deliv Rev. 117 (2017) 86–110, https://doi.org/10.1016/j.addr.2017.07.001.
[53] S.L. Childs, G.P. Stahly, A. Park, The salt−cocrystal continuum: the influence of crystal structure on ionization state, Mol Pharm 4 (2007) 323–338, https://doi.org/10.1021/mp0601345.
[54] A. Aramini, G. Bianchini, S. Lillini, S. Bordignon, M. Tomassetti, R. Novelli, S. Mattioli, L. Lvova, R. Paolesse, M.R. Chierotti, M. Allegretti, Unexpected Salt/Cocrystal Polymorphism of the Ketoprofen-Lysine System: Discovery of a New Ketoprofen–l-Lysine Salt Polymorph with Different Physicochemical and Pharmacokinetic Properties, Pharmaceuticals 14 (2021) 555, https://doi.org/10.3390/ph14060555.
[55] J. Ding, J. Li, S. Mao, Development and evaluation of vinpocetine inclusion complex for brain targeting, Asian J Pharm Sci 10 (2015) 114–120, https://doi.org/10.1016/j.ajps.2014.08.008.
[56] D. Sikorski, K. Gzyra-Jagieła, Z. Draczyński, The kinetics of chitosan degradation in organic acid solutions, Mar Drugs 19 (2021) 236, https://doi.org/10.3390/md19050236.
[57] F. Bravetti, R.E. Russo, S. Bordignon, A. Gallo, F. Rossi, C. Nervi, R. Gobetto, M. R. Chierotti, Zwitterionic or not? fast and reliable structure determination by combining crystal structure prediction and solid-state NMR, Molecules 28 (2023) 1876, https://doi.org/10.3390/molecules28041876.
[58] N. Jagadeesh Babu, A. Nangia, Solubility advantage of amorphous drugs and pharmaceutical cocrystals, Cryst. Growth Des. 11 (2011) 2662–2679, https://doi.org/10.1021/cg200492w.
[59] D.D. Bavishi, C.H. Borkhataria, Spring and parachute: How cocrystals enhance solubility, Prog. Cryst. Growth Charact. Mater. 62 (2016) 1–8, https://doi.org/10.1016/j.pcrysgrow.2016.07.001.
[60] R. Thakuria, A. Nangia, Highly soluble olanzapinium maleate crystalline salts, CrstEngComm 13 (2011) 1759, https://doi.org/10.1039/c0ce00787k.
[61] A.M. Healy, Z. Ayenew Worku, D. Kumar, A.M. Madi, Pharmaceutical solvates, hydrates and amorphous forms: A special emphasis on cocrystals, Adv Drug Deliv Rev. 117 (2017) 25–46, https://doi.org/10.1016/j.addr.2017.03.002.
[62] S.J. Dengale, H. Grohganz, T. Rades, K. Löbmann, Recent advances in co-amorphous drug formulations, Adv Drug Deliv Rev 100 (2016) 116–125, https://doi.org/10.1016/j.addr.2015.12.009.

SUPPLEMENTARY INFORMATION

Enantiospecific crystallisation behaviour of malic acid in mechanochemical reactions with vinpocetine

Ilenia D'Abbrunzo, Rebecca Birolo, Michele R. Chierotti, Dejan-Krešimir Bučar, Dario Voinovich, Beatrice Perissutti, Dritan Hasa

Contents

Table S1. Solubility values of VINPO and MAL in ethyl acetate (EA), ethanol (EtOH), acetone (AcT), acetonitrile (ACN) and hexane (HXN).

	Polarity index	Dielectric constant	VINPO solubility (mg/mL)	MAL solubility (mg/mL)
EA	4.4	6.02	8.7908*	<10.00
EtOH	5.2	24.30	17.52	>10.00
AcT	5.1	20.70	25.00	>10.00
ACN	5.8	37.50	1.00	>10.00
HXN	0	1.89	3.4599*	<0.50

*values reported as molar fraction of solubility

Figure S1. Solution crystallisation results in EA showing the formation of single crystals in case of using VINPO-L-MAL mixture and gels in case of VINPO-D-MAL and VINPO-DL-MAL.

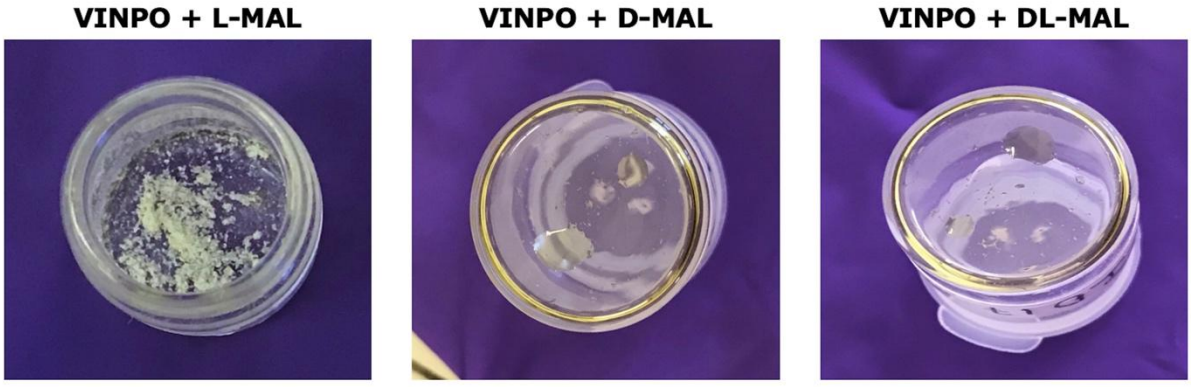

Figure S2. Solution crystallisation results in EtOH showing the formation of single crystals in case of using VINPO-L-MAL mixture and gels in case of VINPO-D-MAL and VINPO-DL-MAL.

Figure S3. Solution crystallisation results in AcT showing the formation of single crystals in case of using VINPO-L-MAL mixture and gels in case of VINPO-D-MAL and VINPO-DL-MAL

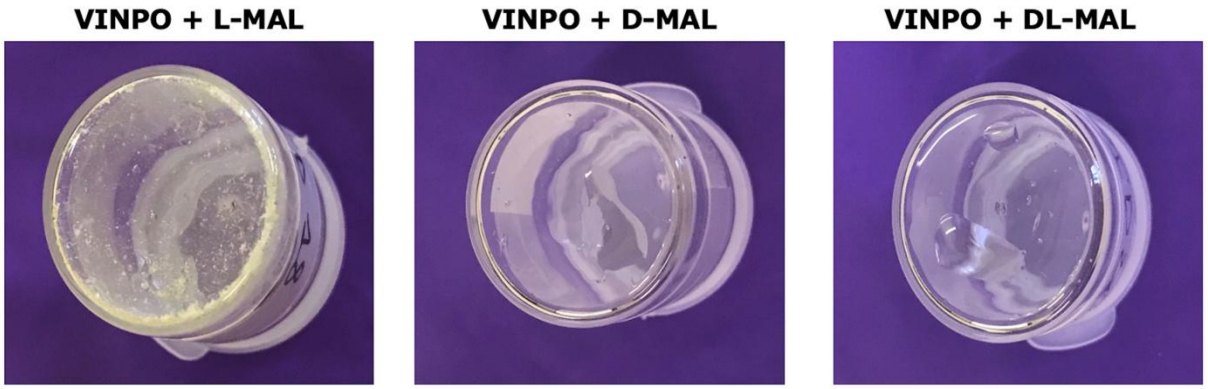

Figure S4. Solution crystallisation results in ACN showing the formation of single crystals in case of using VINPO-L-MAL mixture and gels in case of VINPO-D-MAL and VINPO-DL-MAL.

Table S2. Crystallographic and refinement parameters of VINPO-L-MAL

	VINPO-L-MAL
empirical formula	$C_{26}H_{32}N_2O_7$
M_r / g mol^{-1}	484.53
crystal system	monoclinic
space group	$P2_1$
a / Å	7.53408(4)
b / Å	8.37499(6)
c / Å	19.36915(11)
α / °	90
β / °	95.2625(5)
γ / °	90
V / Å^3	1217.000(13)
Z	2
ρ_{calc} / g cm^{-3}	1.322
T / K	150.0 (1)
μ / mm^{-1}	0.794
F(000)	516
crystal size / mm^3	0.27 × 0.24 × 0.11
radiation	CuK_α (λ = 1.54178 Å)
2θ range for data collection / °	4.574 – 133.400
index ranges	$-9 \le h \le 9$ $-9 \le k \le 10$ $-24 \le l \le 24$
number of collected reflections	44361
unique reflections	4909
number of unique reflections	4818 [$I > 2\sigma(I)$]
R_{int}	0.0402
$R(F)$, $F > 2\sigma$(F)	0.0278
$wR(F^2)$, $F > 2\sigma$(F)	0.0662
$R(F)$, all data	0.0284
$wR(F^2)$, all data	0.0668
Δ_r (max., min.) e Å^{-3}	0.134,−0.134
Flack parameter	-0.05(6)
CCDC deposition number	2346109

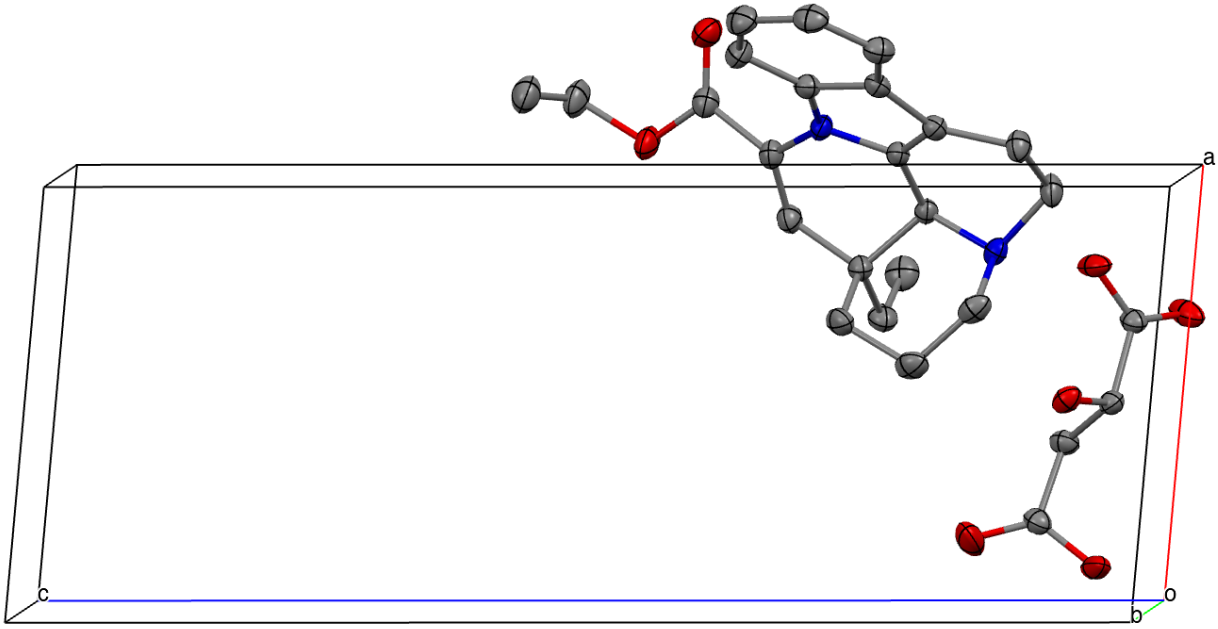

Figure S5. The asymmetric unit of VINPO-L-MAL. The thermal ellipsoids are drawn at the 50% probability level. Colour scheme: carbon – dark grey, nitrogen – blue, oxygen – red. All hydrogen atoms were omitted to enhance the clarity of the figure.

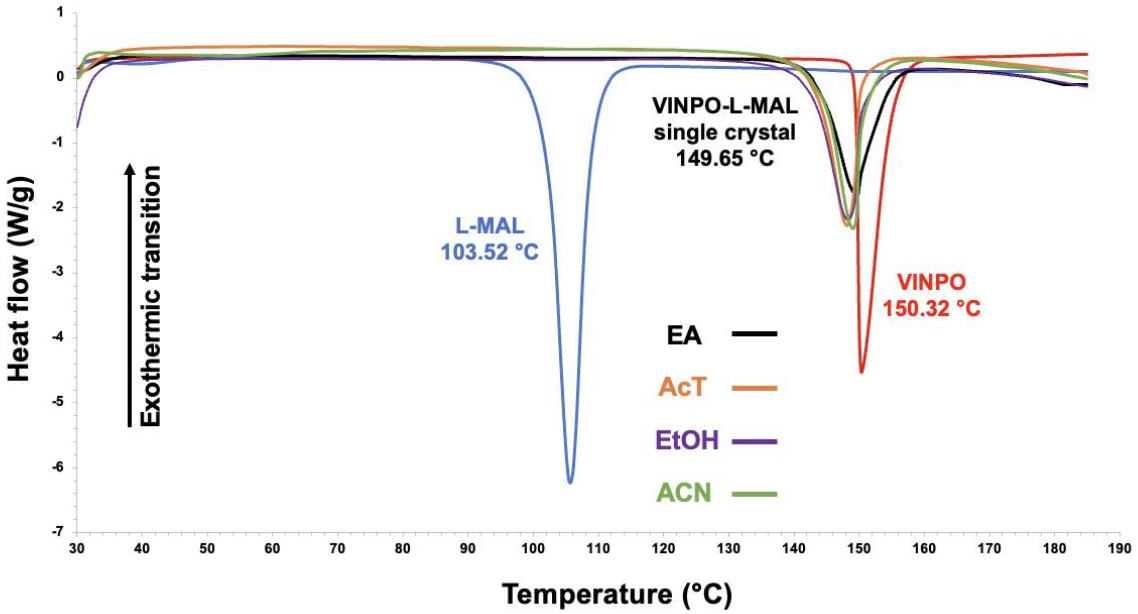

Figure S6. Comparison of DSC curves of single crystals obtained through solution crystallisation in EA, AcT, EtOH and ACN.

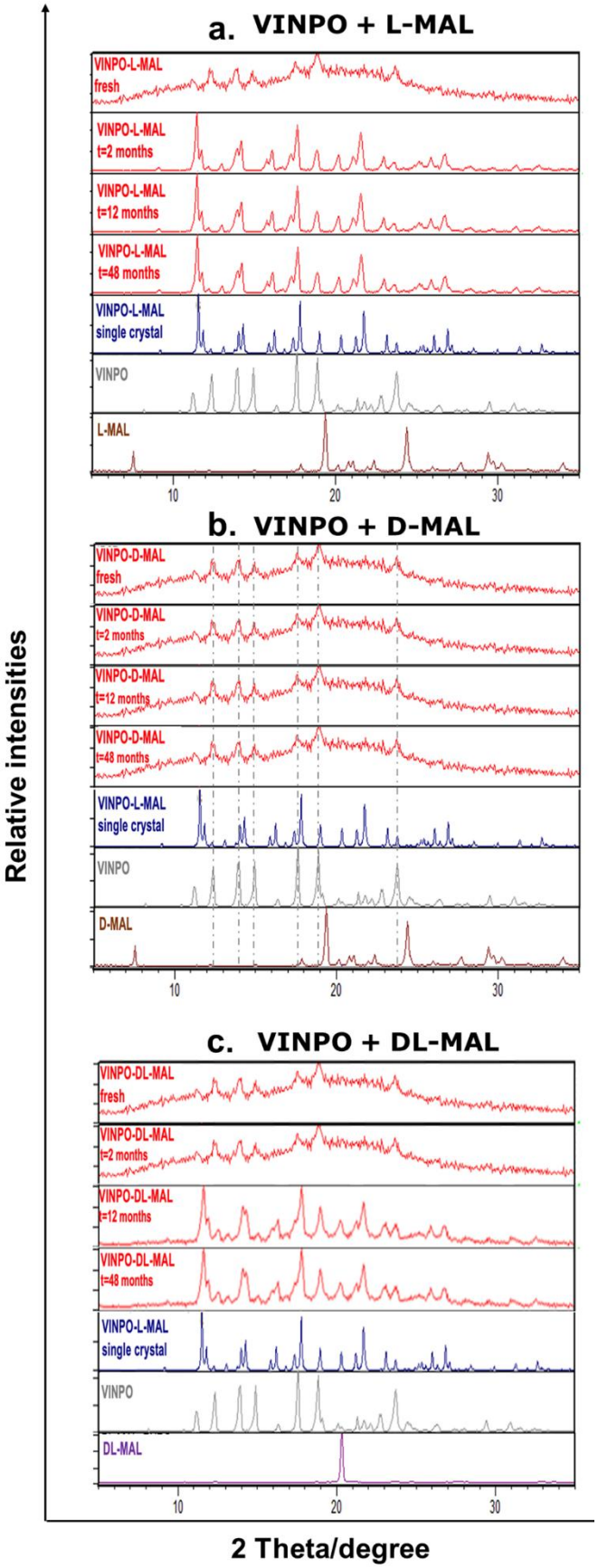

Figure S7. PXRD patterns of NG mechanochemically prepared (a) VINPO-L-MAL, (b) VINPO-D-MAL, (c) VINPO DL-MAL samples, acquired at t=0, t=2 months, t=12 months and t=48 months. Grey dotted lines highlight VINPO reflections.

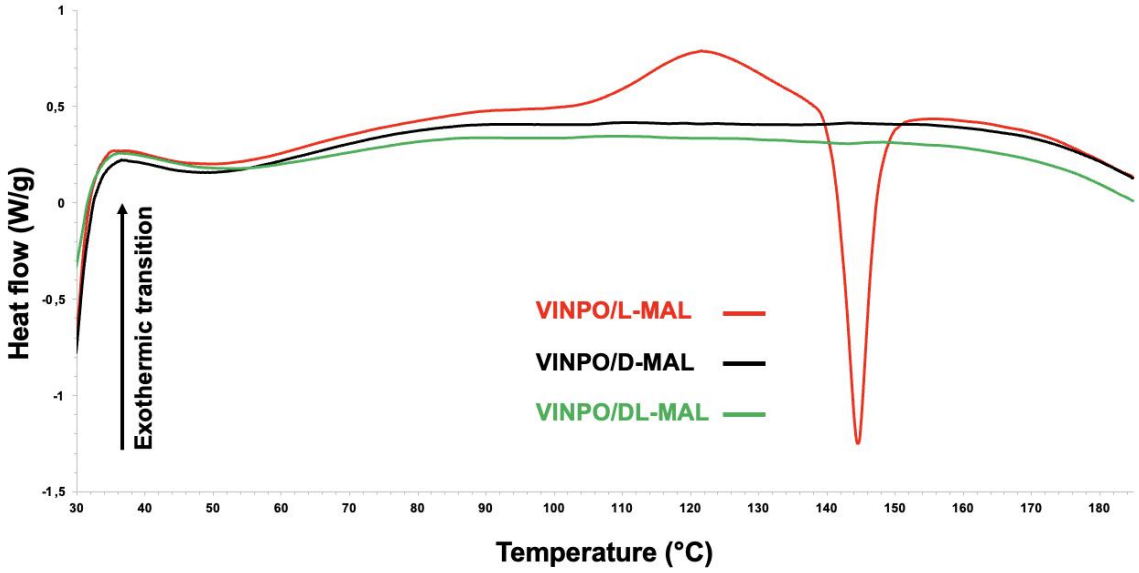

Figure S8. DSC curves of the fresh VINPO-L-MAL, VINPO-D-MAL and VINPO-DL-MAL systems.

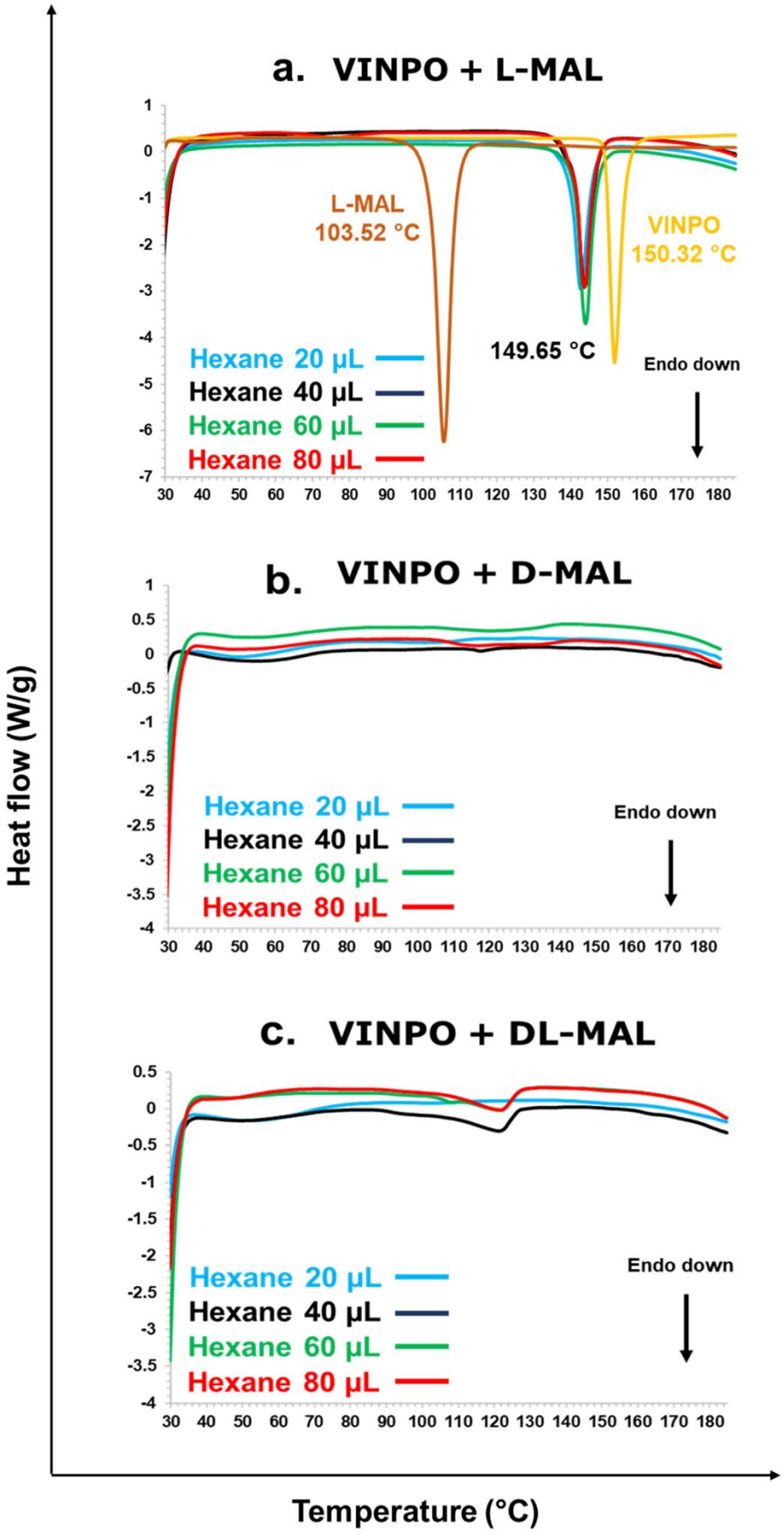

Figure S9. DSC results of LAG experiments with 0.1, 0.2, 0.3, 0.4 η of HXN for (a) VINPO-L-MAL, (b) VINPO-D-MAL and (c) VINPO-DL-MAL three systems.

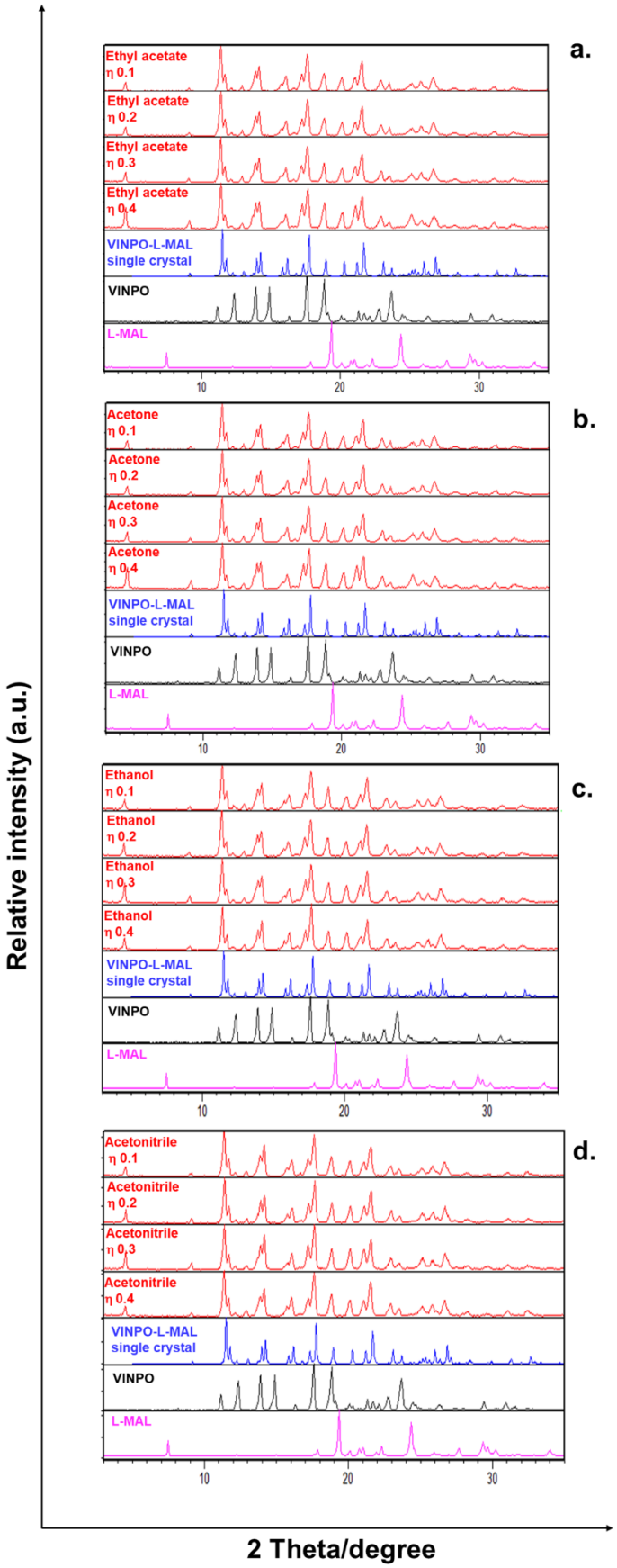

Figure S10. PXRD patterns of LAG experiments of VINPO-L-MAL system with 0.1, 0.2, 0.3, 0.4 η of (a) EA, (b) AcT, (c) EtOH and (d) ACN.

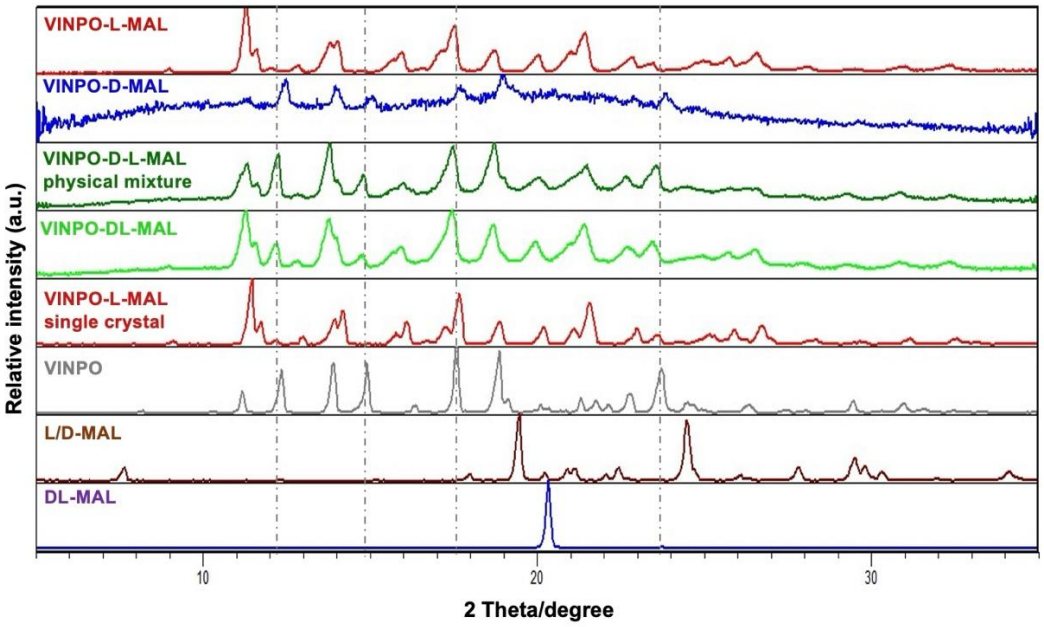

Figure S11. PXRD patterns of LAG experiments of VINPO-L-MAL, VINPO-D-MAL, VINPO D-L-MAL PM, VINPO DL-MAL, plus VINPO-L-MAL single crystal and raw VINPO, raw D/L-MAL and DL-MAL. Grey dotted lines highlight VINPO reflections.

Table S3. Summary of LAG experiments through a schematic representation: green triangles are crystalline products, red triangles amorphous products, / symbol corresponds to not analysed compounds.

	LIQUID-ASSISTED GRINDING																			
	HEXANE				ETHYL ACETATE				ETHANOL				ACETONE				ACETONITRILE			
	20 µL	40 µL	60 µL	80 µL	20 µL	40 µL	60 µL	80 µL	20 µL	40 µL	60 µL	80 µL	20 µL	40 µL	60 µL	80 µL	20 µL	40 µL	60 µL	80 µL
VINPO-L-MAL	▲	▲	▲	▲	▲	▲	▲	▲	▲	▲	▲	▲	▲	▲	▲	▲	▲	▲	▲	▲
VINPO-D-MAL	▲	▲	▲	▲	/	/	/	/	/	/	/	/	/	/	/	/	/	/	/	/
VINPO-DL-MAL	▲	▲	▲	▲	/	/	/	/	/	/	/	/	/	/	/	/	/	/	/	/

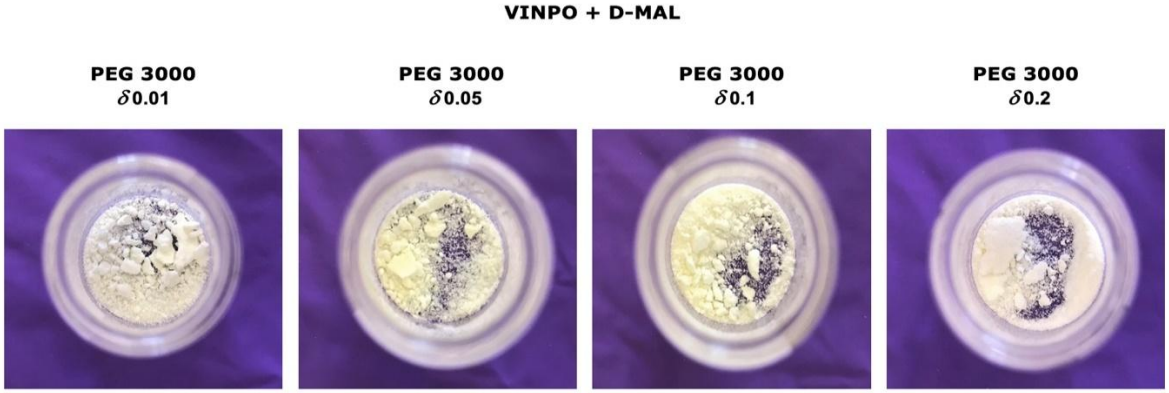

Figure S12. Images of free-flowing VINPO-D-MAL after POLAG experiments with 0.01, 0.05, 0.1, 0.2 δ of PEG 3000.

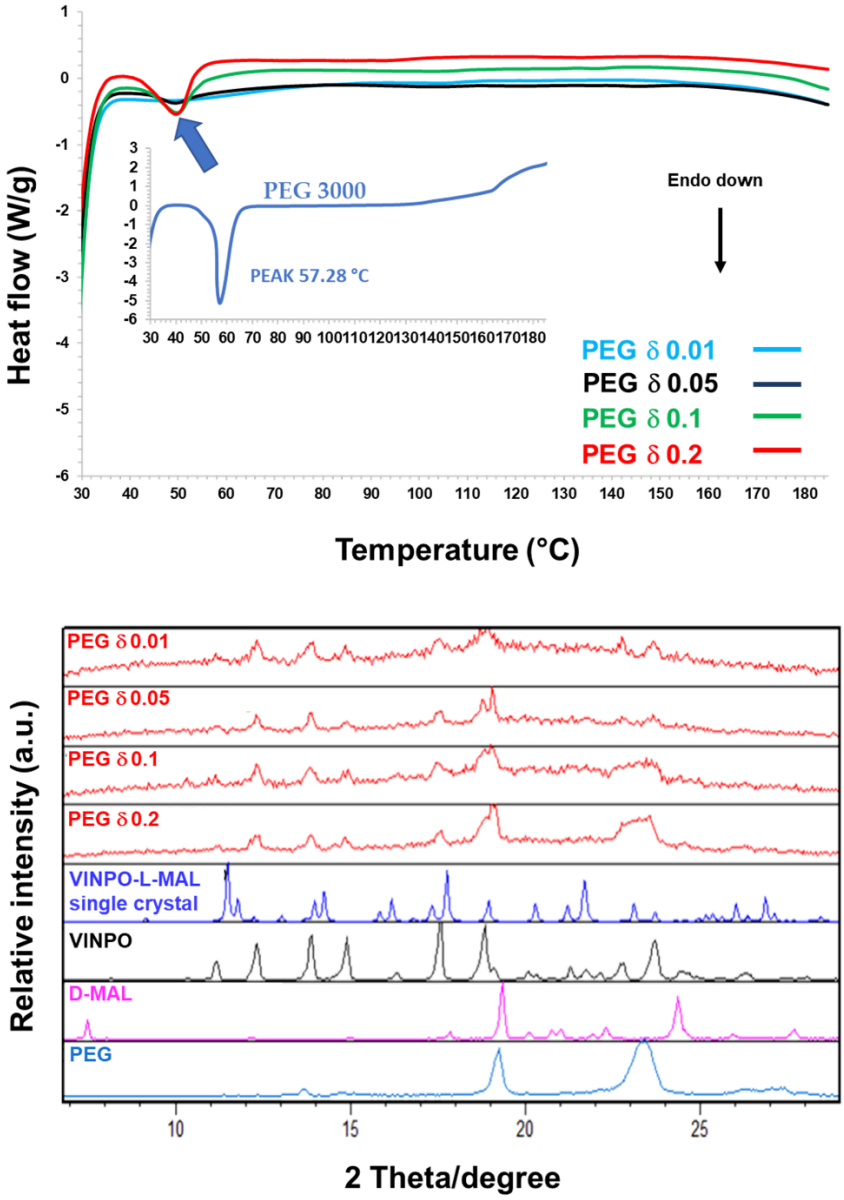

Figure S13. DSC (top) and PXRD (bottom) results of the VINPO-D-MAL system after POLAG experiments with 0.01, 0.05, 0.1, 0.2 δ of PEG 3000.

Figure S14. Images of opened jars showing VINPO-DL-MAL deliquescent material after LAG experiments with (a) EA, (b) AcT, (c) EtOH and (d) ACN.

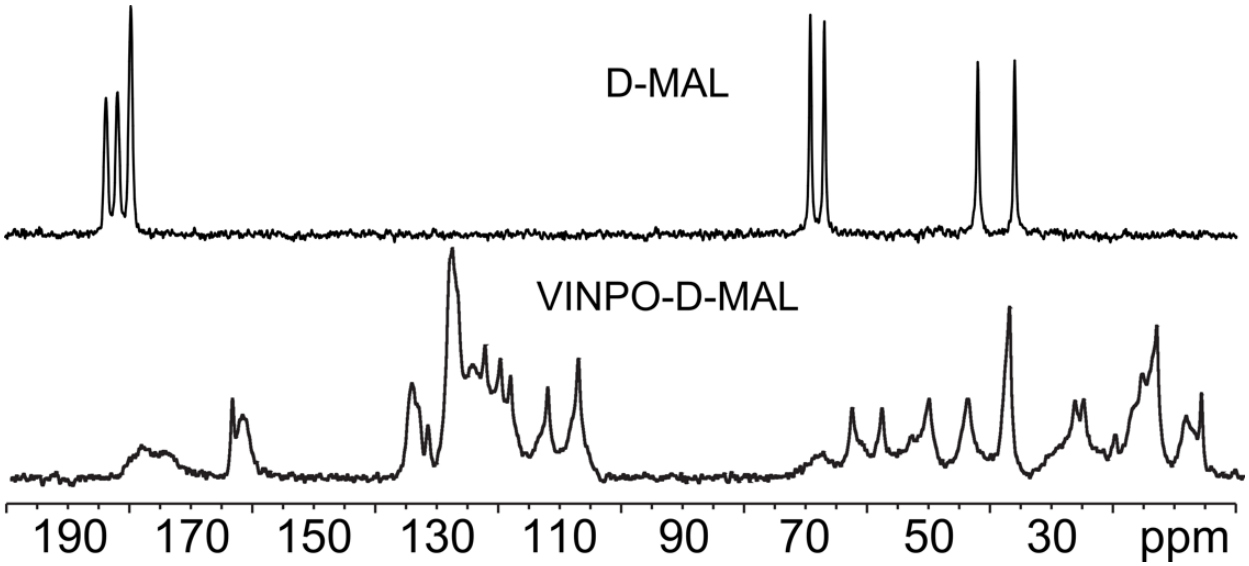

Figure S15. ^{13}C (100.6 MHz) CPMAS spectra of VINPO-D-MAL compared to crystalline D-MAL acquired at a spinning speed of 12 kHz at room temperature.

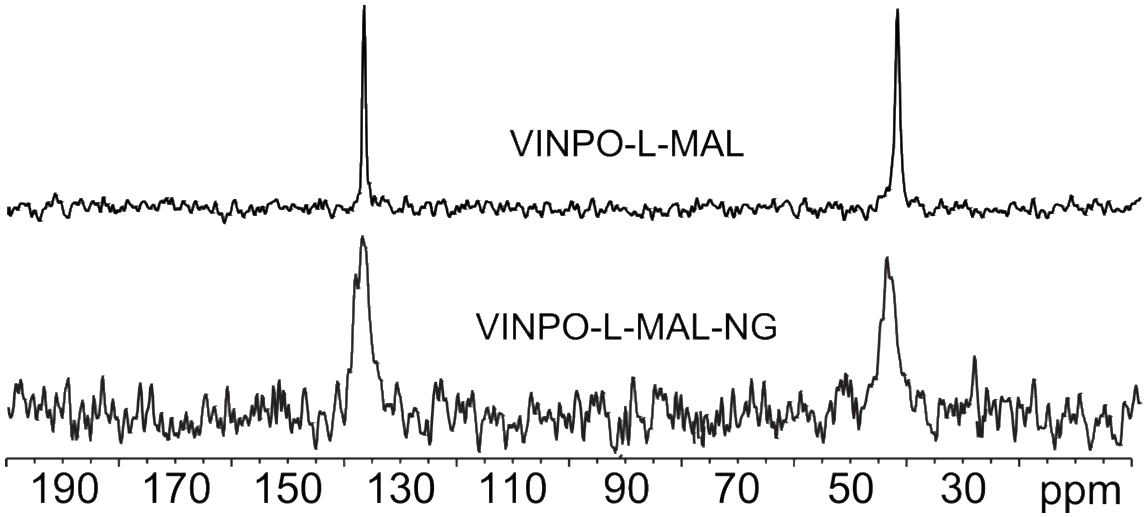

Figure S16. ^{15}N (40.6 MHz) CPMAS spectra of crystalline VINPO-L-MAL and VINPO-L-MAL-NG acquired at a spinning speed of 9 kHz at room temperature.

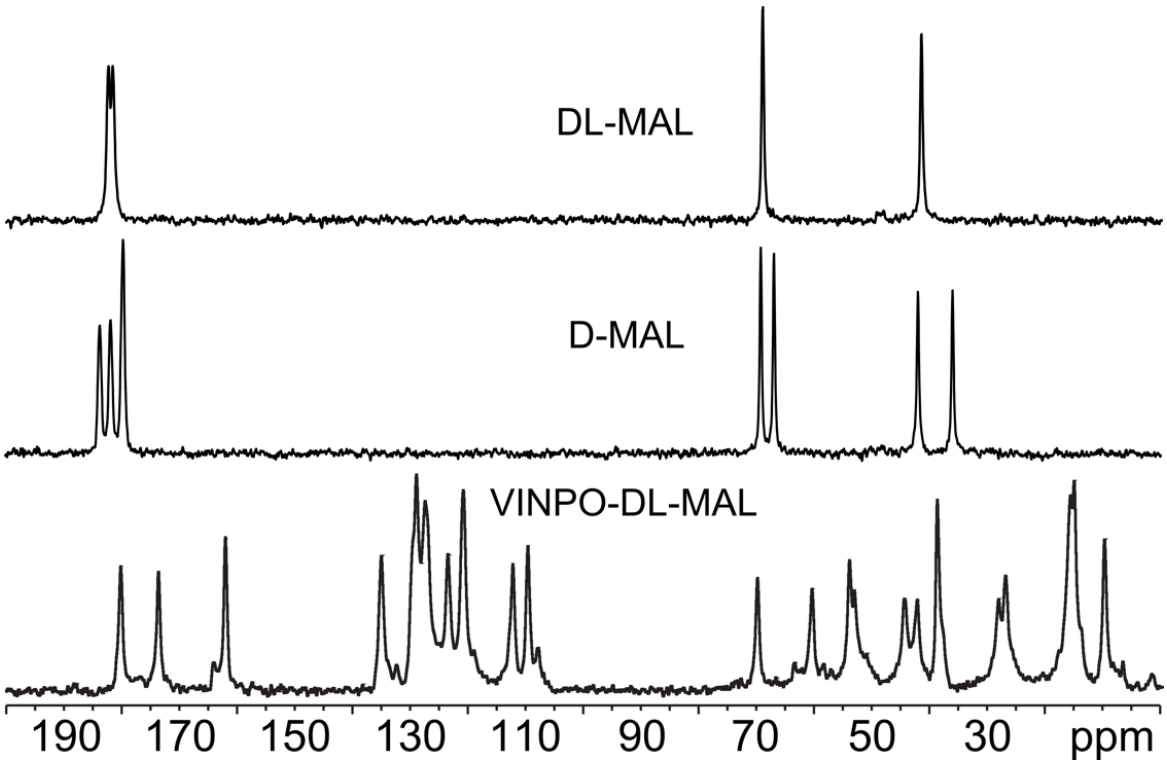

Figure S17. ^{13}C (100 MHz) CPMAS spectra of VINPO-DL-MAL system, compared to crystalline DL-MAL and D-MAL acquired at a spinning speed of 12 kHz at room temperature.